Analysis of the pressure drop through structured packed beds

PJ van Loggerenberg


orcid.org/0000-0003-1035-2811

Mini-Dissertation accepted in partial fulfilment of the requirements for the degree Master of Engineering with Nuclear Engineering at the North-West University

Supervisor: Prof CG du Toit

Graduation: May 2020

Student number: 24087408

ABSTRACT

Accurately analysing the pressure drop over structured packed beds is of great importance to certain reactor designs, such as the Pebble Bed Modular Reactor (PBMR). In previous studies, the High Pressure Test Unit (HPTU) was used to conduct pressure drop experiments for three structured packed beds with separate porosities, designated as the Pressure Drop Test Section (PDTS) experiments, to aid in the design of the PBMR. However, conducting physical experiments to analyse the pressure drop over packed beds is often too expensive and time-consuming. Computational Fluid Dynamics (CFD) offers the possibility to accurately simulate the flow and analyse the pressure drop over structured packed beds. CFD was used to validate the PDTS experiments. Previous attempts at using Computational Fluid Dynamics to simulate the flow and analyse the pressure drop over structured packed beds have not produced methods which can be universally applied. Therefore, the successful simulation of the experiments in this study will require unique methods.

The structured packed beds of the HPTU were replicated using a Computer Aided Design program, and the flow over the beds were simulated using CFD. SolidWorks (2016) was the CAD-program used to generate the packed beds, and Star-CCM+ was used to simulate the flow explicitly. The work done in this study is an extension of preliminary work completed by previous studies. A residual analysis was conducted to establish favourable simulation settings that will reduce the residuals of the momentum, energy and continuity equations to obtain converged solutions. A mesh dependence study was conducted to determine the influence of the mesh fineness on the pressure drop over the bed. Furthermore, the influence of prism layers and the thickness of the prism layers on the pressure drop was also investigated. These investigations formed part of a methodology development. The validity of the methodology was determined by comparing the results of the simulations with experimental results. It was found that it was not possible to accurately simulate the flow over structured packed beds for all required flow conditions, but accurate results were generated for laminar and slightly turbulent flow conditions.

The methodology which was developed during this study could aid in future attempts to simulate the flow of a working fluid over a structured packed bed. The thickness and number of the prism layers was also shown to have an influence on the pressure drop. It was also proven that the HPTU experiments conducted on the Pressure Drop Test Sections can be successfully modelled using CFD.

Keywords: *Computational Fluid Dynamics (CFD); Numerical analysis; Packed bed; Structured; Pressure drop; Porosity*

ACKNOWLEDGEMENTS

I would foremost like to thank my study supervisor, Prof. C.G. du Toit, for his continuous help, patience and guidance through this study, and for making sure my work is on track and offering thoughtful insights into my study, and lastly for offering me the opportunity to be a part of the South African Research Chair Initiative in Nuclear Engineering.

Furthermore, I would also like to thank Ms. Francina Jacobs, who moved earth and heavens to ensure that I received the proper support.

I would also like to Mr. Drikus Vermaak for his support with certain parts of my study, specifically the CFD simulations.

Lastly, I would like to give thanks and praise to my parents, who fully supported and encouraged me through my study to complete it to the best of my abilities.

NATIONAL RESEARCH FOUNDATION DISCLAIMER

This work is based on the research supported by the South African Research Chairs Initiative of the Department of Science and Technology and National Research Foundation of South Africa (Grant Number 61059). Any opinion, finding and conclusion or recommendation expressed in this material is that of the author and the National Research Foundation does not accept liability in this regard.

TABLE OF CONTENTS

LIST OF TABLES

LIST OF FIGURES

NOMENCLATURE

Abbreviations	Meaning
BCC	Body-centred Cubic
CAD	Computer-aided Design
CFD	Computational Fluid Dynamics
CFL	Courant-Friedrichs-Lewy
FCC	Face-centred Cubic
HPTU	High-Pressure Test Unit
HTGR	High-Temperature Gas-cooled Reactor
HTTF	Heat Transfer Test Facility
HTTU	High-Temperature Test Unit
KTA	German Nuclear Safety Standard Commission
LES	Large Eddy Simulation
Ltd.	Limited (company)
PBMR	Pebble Bed Modular Reactor
PDTS	Pressure Drop Test Section/s
Pty.	Proprietary
RANS	Reynolds-Averaged Navier-Stokes
RSM	Reynolds Stress Model
SC	Simple Cubic
SOC	State-Owned Company
TRISO	Tristructural-isotropic

Greek letters	Description
α (-)	Aspect ratio
Γ $(\frac{kg}{m \cdot s})$	Diffusion coefficient
ϵ (-)	Total porosity
ϵ $(\frac{m^2}{s^3})$	Turbulence dissipation rate
ϵ_b (-)	Bulk porosity
κ $(\frac{W}{m \cdot K})$	Thermal conductivity coefficient
μ $(\frac{N \cdot s}{m^2})$	Dynamic viscosity
μ_t $(\frac{N \cdot s}{m^2})$	Turbulent viscosity

ν $(\frac{m^2}{s})$	Kinematic viscosity
ρ $(\frac{kg}{m^3})$	Density
Φ $(\frac{m^3}{s \cdot m^2})$	Fluid flux
ϕ	General property (unit property dependent)
Ψ (-)	Friction factor
Ω $(\frac{W}{m^3})$	Dissipation constant
ω $(\frac{1}{s})$	Specific turbulence dissipation rate

General	**Description**
$A\,(\mathrm{m}^2)$	Flow cross-section
$B\,(\mathrm{mm})$	Base size
$C\,(\text{-})$	Convective Courant number
$D\ (\mathrm{m})$	Cylinder diameter
$D_H\ (\mathrm{m})$	Hydraulic diameter
$d_p\ (\mathrm{m})$	Particle diameter
$i\,(\frac{J}{kg})$	Specific internal energy
k $(\frac{m^2}{s^2})$	Kinetic energy dissipation rate
$L\,(\mathrm{m})$	Bed length
$n\,(\text{-})$	Power Law velocity exponent
N_2	Nitrogen gas
$p\,(\mathrm{Pa})$	Pressure
$\Delta P\ (\mathrm{Pa})$	Pressure drop
$Q\,(\mathrm{m}^3)$	Volumetric flowrate
$R\,(\mathrm{m})$	Cylinder radius
$r\,(\mathrm{m})$	Radial coordinate
$r_p\,(\mathrm{m})$	Particle radius
$Re\ (\text{-})$	Reynolds number
$Re_p\ (\text{-})$	Particle Reynolds number
$Re_m\ (\text{-})$	Modified Reynolds number
S_ϕ	Source term (unit property dependent)
$S_M\,(\frac{N}{m^3})$	Momentum source term
$\Delta t\ (\mathrm{s})$	Time-step

$U(\frac{m}{s})$	Superficial velocity
$u(\frac{m}{s})$	Velocity component in x-direction
$U_i(\frac{m}{s})$	Interstitial velocity
$u^*(\frac{m}{s})$	Reference velocity
$V(m^3)$	Volume
$v(\frac{m}{s})$	Velocity component in y-direction
$V_{avg}(\frac{m}{s})$	Average velocity
$V_{max}(\frac{m}{s})$	Maximum velocity
$V(r)(\frac{m}{s})$	Radial velocity
$w(\frac{m}{s})$	Velocity component in z-direction
$\Delta x\ (m)$	Cell size in meter
y^+ (m)	Wall distance

Vectors	**Description**
$\boldsymbol{T_t}\ (\frac{N}{m^2})$	Reynolds stress tensor
$\boldsymbol{u}\ (\frac{m}{s})$	Velocity vector

Subscripts	**Description**
Blake	Blake (1922)
Ergun	Ergun (1952)
W&T	Wentz and Thodos (1963)
W&T exp	Wentz and Thodos (1963) experimental results
KTA	KTA (1981)
E&S	Eisfeld and Schnitzlein (2001)
Star-CCM+	Results obtained from Star-CCM+ simulations
Experimental	PDTS experimental results
x, y, z	Component in the respective Cartesian directions

Mathematical operators	**Description**
$\int$	Integral
∇	Del operator
$\bar{}$	Average

$'$	Partial derivative
$\frac{\partial}{\partial t}$	Rate of change of respective function or property

Units	**Description**
mm	Millimetre
m	Metre
Pa	Pascal
kPa	Kilopascal
MPa	Megapascal
K	Kelvin
˚C	Degrees Celsius
s	Second
ms	Millisecond
$\frac{m}{s}$, m/s or $m \cdot s^{-1}$	Meter per second

CHAPTER 1: INTRODUCTION

1.1 Background

Pebble bed reactors are used extensively for various purposes, such as absorption towers, ion exchange columns and catalytic reactors (Caulkin, et al., 2007). Pebble bed reactors have also been proposed as a possible configuration for Generation IV nuclear reactors which would amongst others take the form of High-Temperature Gas-cooled Reactors (HTGR) (Hassan, 2008). The thermal-hydraulic properties of a fluid flowing through the pebble beds has been thoroughly researched through the years (Ergun, (1952), Wentz and Thodos (1963), Du Toit and Rousseau (2014), Hassan and Kang (2012)). A demand for safe energy generation has led to the development of the Pebble Bed Modular Reactor (PBMR), which has innate safety properties due to its low power density and large amounts of graphite in the core. Understanding the complex and unsteady flows through a pebble bed is therefore necessary to design and analyse these reactors' cores and requires a wide range of simulation programs and analysis techniques (Hassan & Kang, 2012).

The PBMR concept is derived from the High Temperature Reactor developed by Germany, which forms part of the so-called Generation IV nuclear reactor designs (Hassan, 2008). The PBMR is designed with an annular core surrounded by a graphite reflector, with an additional central graphite reflector. The annular core has inner and outer diameters of 2.0 and 3.7 m, respectively, with a height of 11 m. The core contains approximately 450000 fuel spheres (Latifi & Saeed, 2016). A fuel sphere is made of graphite and contain 9 grams of uranium in thousands of tristructural-isotropic (TRISO) coated particles (Latifi & Du Toit, 2019).

The PBMR SOC (Ltd.) appointed the North-West University, South Africa, in association with M-Tech Industrial (Pty.) Ltd. to design and develop the Heat Transfer Test Facility (HTTF) to generate more extensive thermal-fluid data on packed beds to aid in the development of the PBMR. The HTTF consisted of two units, the High Pressure Test Unit (HPTU) and the High Temperature Test Unit (HTTU). The HPTU and HTTU were associated with detailed sets of integrated and separate effects tests, respectively (Rousseau & van Staden, 2008).

The HPTU was designed to test for the effect of the Nusselt number, fluid effective conductivity and Euler number separately in three separate sets of test sections with distinctive porosities. The applicable span of Reynolds numbers that were used was derived from the anticipated operational conditions of the PBMR reactor operation. The range of Reynolds numbers for the gas flow were specified as low as practically possible, up to a Reynolds number of 48500. This wide range of Reynolds numbers was achieved by conducting the experiments with pure nitrogen,

with the absolute pressure of the nitrogen ranging from 100 kPa to 5MPa, with a temperature for the tests of 35˚C (Rousseau & van Staden, 2008).

The packing structure, amongst other structural parameters, of a pebble bed reactor influences the distribution and shape of the void sizes in the bed, which has an influence on the bed pressure drop. Therefore, the packing method and structure will have an influence on the performance of the reactor. By changing the particle arrangements of structured beds, a direct analysis of its influences can be determined (Du, et al., 2015).

Wentz and Thodos (1963) investigated the effect of the packing structure in packed and distended beds on the pressure drop of a gas flowing through a structured packed bed. The packed and distended beds consisted of five axial sphere layers and had three distinct geometric orientations, namely simple cubic (SC), body-centred cubic (BCC) and face-centred cubic (FCC); with each configuration having separate porosities. The beds were tested for a wide range of modified Reynolds numbers (Re_m), from 2550 up to 64920. These data points were correlated to determine a correlation for the friction factor for both the packed and distended structured beds (Wentz & Thodos, 1963).

In addition to testing for the different effects mentioned previously, the HPTU also tested the pressure drop over structured beds, in tests called the Pressure Drop Test Sections (PDTS). In the PDTS experiments, nitrogen was pumped through three body-centred cubic structured beds consisting of spherical particles. The three beds had three distinct overall porosities of $\epsilon = 0.36$, 0.39 and 0.45, respectively. The overall porosities of the beds were kept constant by fixing the spherical particles to thin cables. The nitrogen was pumped through the beds at fourteen pressure levels, from 100 kPa up to 5000 kPa (pressure levels 1 and 14, respectively). This was done to vary the particle Reynolds number (Re_p) from 1000 to 20000 by changing the density of the nitrogen, whilst keeping the superficial velocity of the nitrogen relatively constant between the experiments. The pressure difference was then measured between the inlet and outlet (Van der Walt, 2006).

1.2 Problem statement

The mechanisms affecting the pressure drop of a fluid flowing through a packed pebble bed are not yet fully quantified. Research on the pressure drop led to various correlations being proposed to predict the pressure drop through a packed bed (Erdim, et al., 2015). These correlations are often dependent on a narrow range of flow and bed structural parameters, limiting their applicability and validity.

The effects that the packing structure has on the pressure drop over a structured packed bed can be determined using computational fluid dynamics (CFD). Wentz and Thodos (1963) conducted experiments to determine the influence of packing structure on the pressure drop of a fluid through a packed pebble bed and developed a correlation to predict the pressure drop. This correlation must be evaluated for its validity and applicability. Furthermore, the High Pressure Testing Unit pressure drop data requires validation using CFD.

1.3 Research aim

The aim of this study is to conduct a grid dependence study for the Wentz and Thodos (1963) simulations (BCC packing structure) to determine the relevant parameters for a grid independent solution using the pressure drop over the bed as the defining metric. Furthermore, the pressure drop through the Pressure Drop Test Sections (PDTS) packed beds of the HPTU must be determined numerically using Star-CCM+. The resultant pressure drops will then be used to calculate the friction factors of the flows. The friction factors will then be compared with those calculated from experimental results and correlations, to verify the validity of the simulations. The aim of this study is to achieve an error percentage of less than 10% between the simulation and experimental results where possible.

1.4 Objectives

The objectives of the first section of this study are as follows:

1. Determine whether the structured packed bed built in SolidWorks 2016 by Van der Merwe (2014) is a good representation of the body-centred cubic packed bed with a porosity of $\epsilon = 0.36$ constructed by Wentz and Thodos (1963).
2. Verify the results obtained by Van der Merwe (2014) in STAR-CCM+ version 7 by using similar simulation settings in STAR-CCM+ version 12.
3. Conduct residual analysis to establish suitable simulation settings that will reduce the residuals and obtain converged solutions.
4. Conduct a mesh dependence study to determine a suitable base size for the mesh.
5. Compare the friction factors calculated from the simulated pressure drops over the packed beds with those calculated from correlations and practical experiments conducted by Wentz and Thodos (1963).

The objectives for the second part of this study are as follows:

1. Conduct residual analysis to establish suitable simulation settings that will reduce the residuals and obtain converged solutions.
2. Validate PDTS experimental data by performing simulations according to the PDTS experimental parameters conducted for porosities of 0.36, 0.39 and 0.45 at three pressure levels: 4 (400 kPa), 7 (700 kPa) and 11 (2000 kPa) out of the fourteen experimental pressure levels, respectively.

1.5 Research Overview

This study is an extension from the work done by Van der Merwe (2014), as well as an extension of the work done by Vermaak (2019). For the former, the geometry developed by Van der Merwe (2014) was tested for mesh dependence over a wide range of Reynolds numbers. For the latter, the geometry developed by Vermaak (2019) was used to validate the pressure drops obtained from the HPTU by Du Toit and Rousseau (2014). Symmetry boundary condition assumptions were chosen similar to those of Vermaak (2019), to reduce the computational resources required. Vermaak (2019) also conducted a mesh independence study, therefore the base size of the mesh was chosen according to his recommendations.

Evaluation of the facets of these studies were done by conducting in-depth analyses on residuals, pressure drops and their resultant friction factors. The friction factors were also calculated using various correlations proposed in the literature and the different results were then compared with each other.

1.6 Limitations and assumptions

This study is limited to the pressure drop over body-centred cubic packed pebble beds. The effect of heat transfer from the pebbles and walls was not considered. Therefore, only adiabatic and iso-thermal flow through the voids in the packed beds was modelled.

CHAPTER 2: LITERATURE SUMMARY

Several theoretical correlations to predict the pressure drop over a packed bed have been proposed (Ergun (1952), Wentz and Thodos (1963), KTA (1988), Eisfeld and Schnitzlein (2001)). These correlations have been proven to be valid for specific structural and flow conditions but fail to give results which compare favourably to experimental values when applied to structured beds over a large range of flow conditions. Complete understanding of the flow of the fluid through the packed bed as well as its various mechanical and fluid properties have been hampered by the complex geometrical properties of structured packed beds.

A literature survey was undertaken with the goal of understanding the influence that various parameters have on the pressure drop of a fluid flowing through a structured packed bed with spherical particles. The parameters affecting the pressure drop over a packed bed which have been studied most frequently in literature include the aspect ratio, void fraction, structuredness, wall effect, particle size and flow regime.

2.1 Influence of structural parameters on the pressure drop over a packed bed

The structural parameters of a packed bed and their respective influences on the pressure drop will be discussed in this section.

2.1.1 Aspect ratio

The aspect ratio is defined as the ratio of the cylinder diameter to the particle diameter:

$$\boldsymbol{\alpha = \frac{D}{d_p}} \qquad (\mathbf{2.1})$$

Where α is the aspect ratio, D is the cylinder diameter, and d_p is the particle diameter. It should be noted that the definition for the aspect ratio in Eq. (2.1) may only be applied to packed beds with cylindrical cross-sections which consist of mono-sized particles.

Handley and Heggs (1968) studied the effect of the aspect ratio on the pressure drop of a gas flowing through a packed bed for $1 \leq Re_m \leq 7500$. The packed beds used in their tests had aspect ratios varying between 8 and 22. During testing, Handley and Heggs (1968) observed that the aspect ratio had a negligible effect on the pressure drop through a packed bed (Handley & Heggs, 1968).

The Brinkman equation was used to show that the pressure drop decreases with a decrease in aspect ratio due to maldistribution, whilst wall-friction has the effect of increasing pressure drop

with a decrease in aspect ratio (Winterberg & Tsotsas, 2000). Raichura (2010) used experiments to show that the coefficients of the Ergun equation, which can be used to predict the pressure drop, are largely functions of the aspect ratio, with a low aspect ratio allowing for an increase in the wall effect due to a larger void fraction near the wall (Raichura, 2010). It should be noted that the aspect ratio contributes largely to the various void fraction factors, such as void fraction distribution (axially and radially (Du Toit, 2008)), and it has been shown that these factors are some of the most important influences on the pressure drop (Du, et al., 2015).

Ribeiro et al. (2010) conducted experiments to discern the influence of the aspect ratio on the pressure drop through a packed bed in the laminar and transitional flow regimes. The pressure gradient against the particle Reynolds number for four separate aspect ratios are shown in Figure 2.1-1:

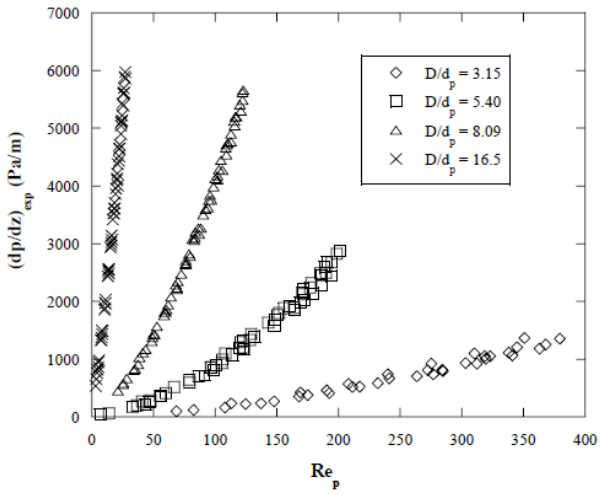

Figure 2.1-1: Pressure gradient versus particle Reynolds number for constant aspect ratios (Ribeiro, et al., 2010)

From Figure 2.1-1, an increase in the aspect ratio of the packed bed results in a larger pressure gradient over the bed (Ribeiro, et al., 2010). This means that the pressure drop is inversely proportional to the aspect ratio. This observation is confirmed by Hassan and Kang (2012), who tested the pressure drop over randomly packed beds with three different porosities at high Reynolds numbers. Their experimental results are shown in Figure 2.1-2:

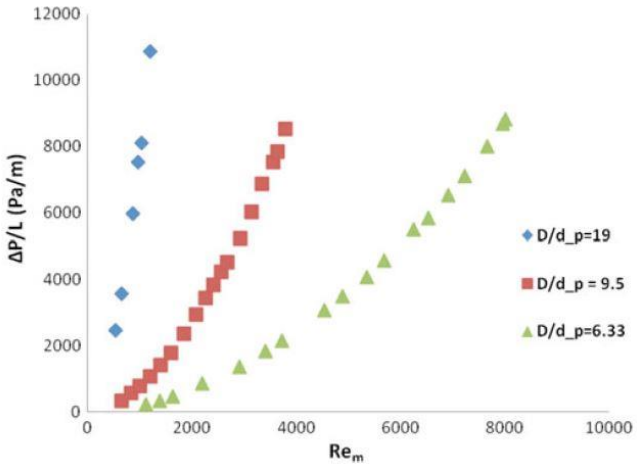

Figure 2.1-2: Pressure drop per unit length versus the modified Reynolds number (Hassan & Kang, 2012)

Figure 2.1-2 shows the pressure drop per unit length against the modified Reynolds number for beds with three aspect ratios obtained by Hassan and Kang (2012). It is apparent that the shape of the curves are similar to those obtained by Figure 2.1-1. Therefore, it is confirmed that the pressure gradient is directly proportional to the aspect ratio for a packed bed of spherical particles (Hassan & Kang, 2012).

2.1.2 Porosity

The porosity, or void fraction, of a packed bed or porous medium refers to the fraction of the total volume of the bed which is empty, or void. These voids are the spaces through which the gas flows through the packed bed. The overall porosity can thus be defined as:

$$\varepsilon = \frac{V_{void}}{V_{total}} = 1 - \frac{V_{spheres}}{V_{total}} \tag{2.2}$$

Several papers have been published to explain the influence of the porosity on the pressure drop and friction factor of a fluid flowing through a packed bed [(Blake, 1922), (Ergun, 1952), (KTA, 1981)]. Blake (1922) was the first to characterize the effect of the porosity on the friction factor due to energy losses of the fluid as it flows through the bed.

The equations proposed by Blake (1922) was considered by Ergun (1952) to describe the energy losses, and thus the pressure drop, most effectively at all flow rates. Ergun (1952) tested the effect of the porosity, as well as the particle size, shape and roughness, on the pressure drop of a fluid flowing through a packed bed; using beds of randomly packed spheres with similar porosities. This led Ergun to derive a correlation to predict the pressure drop through a randomly packed bed, which described both the viscous energy losses the kinetic energy losses of a fluid

flowing through a randomly packed bed. This has become known as the Ergun equation, and is still considered a definitive correlation for predicting the pressure drop of a fluid through a packed bed. However, Ergun based his formulation on randomly packed beds, meaning that he did not consider the effect a structured packed bed will have on the pressure drop (Ergun, 1952).

Achenbach (1995) investigated the influence that a change in the porosity would have on the pressure drop through a packed bed. The results of the experiments are shown in Figure 2.1-3:

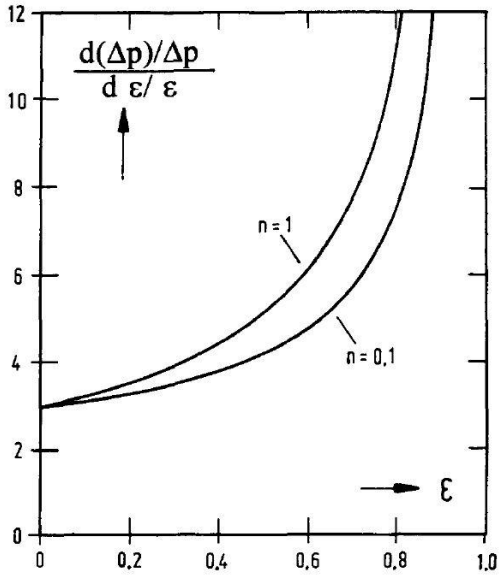

Figure 2.1-3: Sensitivity of the pressure drop to a change in porosity (Achenbach, 1995)

From Figure 2.1-3, it can be seen that the pressure drop is less sensitive to a change in porosity at low porosities; whilst at high porosities, the pressure drop becomes more sensitive to a change in the porosity, where $n = 1$ indicates laminar flow, and $n = 0.1$ indicates turbulent flow. (Achenbach, 1995).

This suggests that accurately measuring or predicting the porosity of a bed is of import when conducting pressure drop experiments. Achenbach (1995) showed that at a porosity of 0.4, a 1% error in calculating the porosity results in an error of 4% in the pressure drop (Achenbach, 1995).

Du Toit and Rousseau (2014) conducted experiments to isolate the effects of the porosity on the pressure drop of a fluid flowing through structured packed beds, called the Pressure Drop Test Sections (PDTS). The experiments were conducted on three test sections with body-centred cubic structure (BCC) packings with square cross-sections, which had porosities of 0.36, 0.39 and 0.45, respectively. The porosities were obtained and maintained by mounting the spheres on cables and varying the distance between the spheres, both laterally and axially. The pressure drop was measured for a range of Reynolds numbers, from $1000 < Re < 50000$. Additionally, Du Toit and

Rousseau (2014) also tested two randomly packed beds, namely the Small Cylindrical Packed Bed (SCPB) and the Small Annular Pebble Bed (SAPB), with porosities of $\epsilon = 0.393$ and $\epsilon = 0.405$ respectively, over the same range of Reynolds numbers as the structured beds. The friction factors calculated from the experiments are shown in Figure 2.1-4, where they are also compared to the Wentz and Thodos (1963), the KTA (1981) and Eisfeld and Schnitzlein (2001) friction factor correlations:

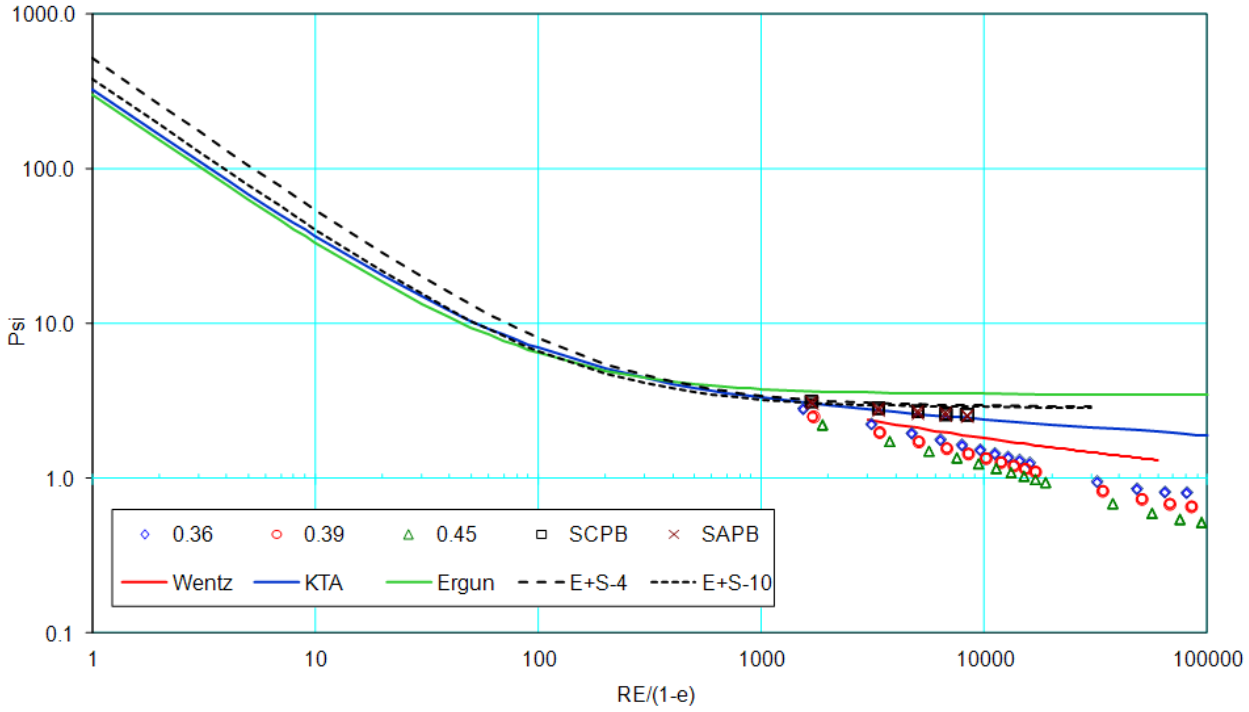

Figure 2.1-4: Experimental results for the friction factor compared to the values predicted by various correlations (Du Toit & Rousseau, 2014).

The empirical correlations proposed by Blake (1922), Ergun (1952), the KTA (1981) and Eisfeld and Schnitzlein (2001) are all based on random packed beds. In Figure 2.1-4 it can be seen that in the case of the structured PDTS beds, the porosity has a significant effect on the friction factor, where the bed with the smallest porosity had the largest friction factor, and the bed with the largest porosity had the lowest friction factor, and by extension, the lowest pressure drop. This indicates that the porosity and the pressure drop are inversely proportional to one another, with a larger porosity bed providing less resistance to the fluid flowing through it than a bed with a smaller porosity. From Figure 2.1-4, it can also be seen that the SAPB and SCPB, are in close agreement to the KTA (1981) and Eisfeld and Schnitzlein (2001) friction factor correlations, which are based on randomly packed beds.

2.1.2.1 The wall effect

The effect that the confining walls have on the packed bed structure in the wall region is significant regardless of packing type. In packed beds of spherical particles, the wall region is defined as the region half a particle diameter to the centre of the bed in the radial direction (Van Antwerpen, et al., 2010). De Klerk (2003) showed that the radial porosity increased dramatically in the wall region, as can be seen in Figure 2.1-5:

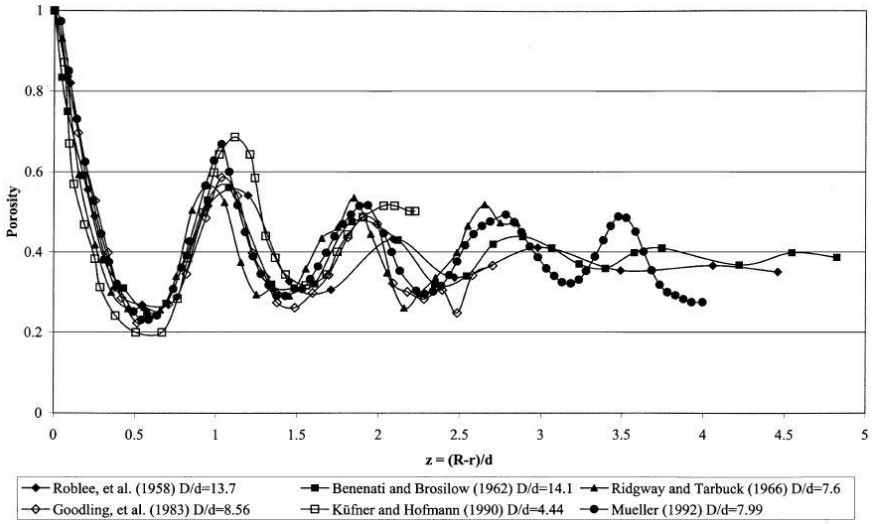

Figure 2.1-5: Radial variation in the porosity as a function of the distance from the wall (De Klerk, 2003)

This increase in porosity is caused by the particles having to arrange themselves close to the wall differently than the overall structure in the bulk region of the packed bed (Di Felice & Gibilaro, 2004). The increase in the porosity at the wall causes a bypass effect in the wall region, which can contribute to errors in determining and predicting the hydrodynamic properties of a certain packing. Several studies found that the wall effect is directly influenced by the aspect ratio, α, as well as flow conditions (Eisfeld & Schnitzlein, 2001). The relation to the aspect ratio can be derived from Equation (2.1), where:

$$\alpha = \frac{D}{d_p} = \frac{2R}{2r_p} = \frac{R}{r_p} \tag{2.3}$$

Therefore, the inverse of the aspect ratio, $\frac{1}{\alpha}$ is an indication of the relative size of the wall region.

Mehta and Hawley (1969) used water flowing through a packed bed with aspect ratios ranging from 7:1 to 90:1 to determine the effect that the confining walls have on the pressure drop and subsequently the friction factor. It was found that for $\alpha \geq 50$, the influence that the containing wall has on the pressure drop is negligible. However, the wall effect has a more pronounced effect on

the pressure drop as the aspect ratio decreases from 50 due to wall friction (Mehta & Hawley, 1969).

Eisfeld and Schnitzlein (2001) analysed more than 2300 experimental data points to determine whether the Reynolds number also influenced the wall effect. These data points covered a wide range of both aspect ratios and Reynolds numbers. Nield (1983) stated that the wall has two counteracting effects on the flow: as mentioned above, the bypass effect causes the local flowrate to increase; whilst the wall also causes the local velocity to decrease to zero due to friction, with no clear indication to which effect is the dominant one. Eisfeld and Schnitzlein (2001) proposed that the dominant effect between the bypass effect and wall friction is dependent on the Reynolds number: the wall friction stretches far from the walls into the packed bed, therefore dominating in the laminar flow regime. On the contrary, the wall friction is confined to a small boundary layer at higher Reynolds numbers, so that the increase in local flowrate due to the bypass effect becomes the dominant effect in the turbulent regime (Eisfeld & Schnitzlein, 2001).

2.1.3 Packing structure

Wentz and Thodos (1963) attempted to characterize the effect that the packing configuration has on the pressure drop of a fluid flowing through a packed bed. In their study, beds of plastic spheres in different geometric configurations with varying porosities were placed inside a cylindrical wind tunnel, where air was passed through the bed. The geometric configurations and their respective porosities are shown in Table 2.1-1:

Table 2.1-1: Orientations and respective porosities of Wentz and Thodos (1963) structured packed beds pressure drop experiments (Wentz & Thodos, 1963)

Orientation	**ε**		
Cubic	0.450	0.729	0.882
Body-centred cubic	0.354	0.615	0.728
Face-centred cubic	0.743		

Wentz and Thodos (1963) made use of (close) packed and distended beds. The spheres were distended by using wires, which made it possible to achieve the high porosities as shown in Table 2.1-1. The wall effect was reduced by cutting the packing into a cylindrical shape and pushing it into the wind tunnel, and each of these geometric configurations and porosities were tested for a wide range of modified Reynolds numbers to increase the accuracy of the results. The experimental data from the cubic, face-centred cubic and body-centred cubic packing structures all converged to a single line when the friction factor was calculated, leading Wentz and Thodos (1963) to propose that their friction factor correlation is valid for all geometric packings.

Susskind and Becker (1967) also investigated the effect of a structured packing on the pressure drop over a packed bed of spheres. Eleven different packed beds were used, all with the same rhombohedral structure, while the bed voidage, spacing between the spheres (both horizontal and vertical), sphere diameter and bed length were varied. They determined that the horizontal spacing between the spheres, which causes continuous flow channels to form, causes the pressure drop to decrease over the bed. Susskind and Becker (1967) also found that beds with the same porosity, but different lateral sphere spacings, had vastly different pressure drops, suggesting that packing structure is of more importance to the pressure drop than porosity (Susskind & Becker, 1967).

Yang et al. (2010) also studied the effect of different geometric configurations of packed beds on the heat transfer and flow properties by using Computational Fluid Dynamics. The geometry used consisted of a square channel that had a length 10 times the particle diameter, with the bed length being eight particle diameters. Yang et al. (2010) firstly conducted tests to compare the hydrodynamic properties of the cubic, face-centred cubic and body-centred cubic configurations. When the pressure drops as a function of Reynolds number for the configurations that were compared, the pressure drop through the simple cubic configured bed was the lowest, and the face-centred cubic configuration was the highest. It was theorized that this was because the tortuosity of the face-centred cubic configuration would be the highest between the three configurations, which would increase the pressure build-up upstream of the bed (Yang, et al., 2010).

As mentioned in Section 2.1.2, Du Toit and Rousseau (2014) tested structured packed beds (of BCC configuration) over a wide range of Reynolds numbers, as well as randomly packed cylindrical and annular beds. As can be seen in Figure 2.1-4, the two randomly packed beds had higher friction factors than the structured packed beds. This can be due to the ordered configuration of the particles in a structured packed bed causing a channelling effect, which would decrease local velocity and lead to an increase in the pressure differential over the packed bed.

2.1.4 Particle size

Several attempts have been made to determine the influence of the particle size on the pressure drop over a packed bed. Abou-Sena et al. (2013) used a rectangular packed bed with glass spheres with varying diameter ranges. These ranges are shown in Table 2.1-2:

Table 2.1-2: Pebble diameters used to determine pebble size influence on pressure drop (Abou-Sena, et al., 2013)

Name	Pebble diameter (mm)	Porosity
S1	0.25 – 0.5	0.61
S2	0.5 – 0.75	
S3	0.75 – 1	
S4	0.9 – 1.2	

As shown in Table 2.1-2, the porosity was kept constant for all four beds. The inlet pressure of the gas flowing over the bed was varied between 2500 and 3800 mbar. The results are shown in Figure 2.1-6 to Figure 2.1-8:

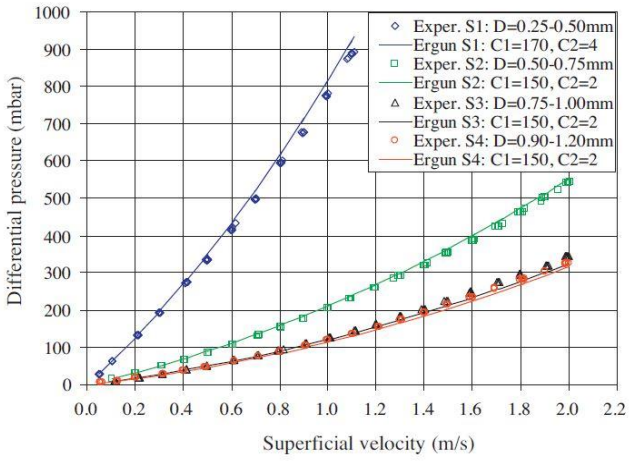

Figure 2.1-6: Pressure drop values of S1 – S4 at 3800 mbar (Abou-Sena, et al., 2013)

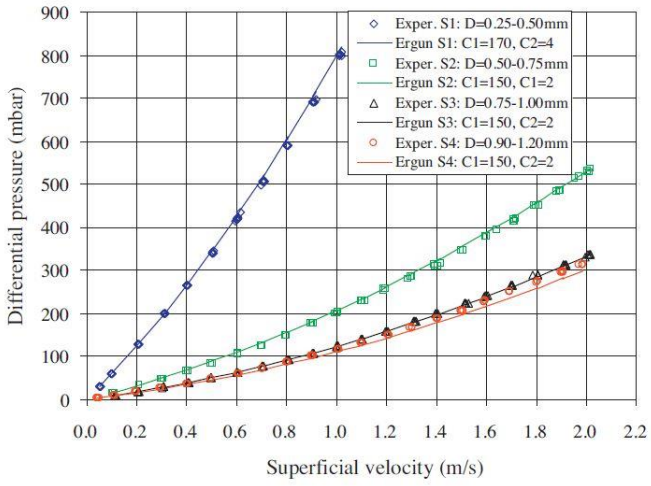

Figure 2.1-7: Pressure drop values of S1 – S4 at 3500 mbar (Abou-Sena, et al., 2013)

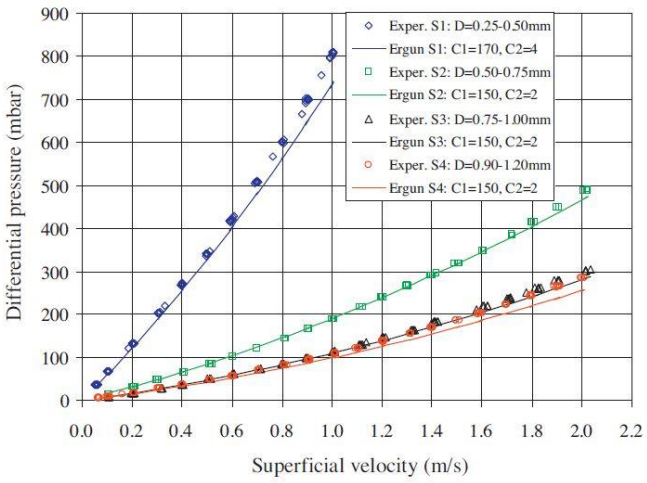

Figure 2.1-8: Pressure drop values of S1 – S4 at 2000 mbar (Abou-Sena, et al., 2013)

From the data presented in Figure 2.1-6 to Figure 2.1-8, Abou-Sena et al. (2013) noticed that the pressure drop increased with a decrease in pebble diameter; and that the pressure drop significantly decreases between S1 and S2, with a smaller decrease between S2 and S3, with only a very small difference between S3 and S4. They also found that for the smallest pebble diameter range, S1, the superficial velocity could not be increased beyond 1 m/s due to the resistance of the bed (Abou-Sena, et al., 2013).

2.2 Flow regimes in packed beds

Rose (1945) experimentally showed that the curve correlating the Reynolds number to the friction factor of a fluid flowing over a bed packed consisting of spherical particles is similar in shape to the curve of the same relation for a single sphere in turbulent flow (Rose, 1945). Furthermore, it was shown by various authors that the flow regime in the packed bed can be better described by relating it to flow over a particle (Rose (1945), Calis (2001)). This is known as the particle Reynolds number, Re_p, which is defined as:

$$Re_p = \frac{\rho U d_p}{\mu} \tag{2.4}$$

Also, of importance when considering the flow through packed beds is the modified Reynolds number, which is the particle Reynolds number over the solid fraction of the bed:

$$Re_m = \frac{Re_p}{1-\epsilon} \tag{2.5}$$

Where in Eq. (2.4), ρ is the density of the working fluid, U is its superficial velocity (based on the volumetric flowrate through the bed cross-sectional area), d_p is the particle diameter and μ is the fluid viscosity. Ziólkowska & Ziólkowski (1988) showed that the flow is viscous (or laminar) for $Re_p < 10$, and that it starts transitioning to turbulent flow between $10 \leq Re_p \leq 300$ and becomes fully turbulent for $Re_p > 300$ (Ziólkowska & Ziólkowski, 1988). However, Seguin et al. (1998) conducted experiments where it was determined that the laminar flow regime extends up to roughly $Re_p \approx 180$. However, there is no general agreement on the Reynolds number for the flow regimes in a packed bed.

Another important parameter related to flow through a packed bed is the interstitial velocity, U_i. The interstitial velocity is simply the ratio of the superficial velocity to the porosity, and is therefore always larger than the superficial velocity, as can be derived from Eq. (2.6):

$$U_i = \frac{U}{\epsilon}\ m \cdot s^{-1} \tag{2.6}$$

Therefore, the interstitial velocity describes the local velocity between the spheres. Suekane, et al. (2003) studied the interstitial velocity distribution in a simple packed bed by using magnetic resonance imaging (MRI) to measure the velocity in real-time. They showed that the maximum fluid velocity was achieved in the centre of the space between the spheres in all flow regimes. Furthermore, it was found that a backflow of up to 0.5 the interstitial velocity was formed close to where the spheres make contact. The velocity of the fluid close to the spheres was relatively low compared to that in the void over all flow regimes. This is due to the viscous forces that are present close to the spheres as well as the wall (Suekane, et al., 2003).

2.3 Pressure drop predictions

The prediction of the pressure drop over a packed bed has been investigated in both theoretical and experimental studies, which sought to describe the influence of the flow and structural parameters on the pressure drop. A common method used to predict and explain the pressure drop is to derive correlations from data obtained through practical experiments.

Blake (1922) was the first to calculate and correlate the pressure drop over a packed bed by using the so-called hydraulic diameter concept, therefore making the flow over the bed analogous to that through a pipe. Two dimensionless equations were used to describe the pressure drop of a working fluid over a packed bed (Blake, 1922):

$$\Psi = \frac{\Delta P}{\rho U^2} \cdot \frac{d_p}{L} \cdot \frac{\epsilon^3}{1-\epsilon} \tag{2.7}$$

And

$$\Psi = \frac{\Delta P}{\rho U_i^2} \cdot \frac{D_H}{L} \tag{2.7a}$$

With ΔP the pressure drop, U the superficial velocity, ρ the density, d_p the particle diameter, L the length of the bed, ϵ the porosity, U_i the interstitial velocity, and D_H the hydraulic diameter. It should be noted that Eqs. (2.7) and (2.7a) do not consider that the pressure drop through a packed bed is simultaneously influenced by kinetic and viscous losses.

Reynolds (1900) developed the first correlation to describe the energy losses that a flowing fluid experiences as it flows through a pipe:

$$\frac{\Delta P}{L} = a\mu U + b\rho U^n \tag{2.8}$$

Where the term $a\mu U$ describes the viscous energy losses, $b\rho U^n$ the kinetic energy losses and $n = 2$ (Ergun, 1952). Ergun (1952) modified the Reynolds correlation to describe the pressure drop through a randomly packed bed, which considers both the viscous and kinetic energy losses:

$$\frac{\Delta P}{L} = a \cdot \frac{(1\text{-}\epsilon)^2}{\epsilon^3} \mathrm{U} + b \cdot \frac{(1-\epsilon)}{\epsilon^3} \rho U^2 \tag{2.9}$$

Where

$$a = 150 \tag{2.9a}$$

And

$$b = 1.75 \tag{2.9b}$$

As with the Reynolds correlation, the second term of the equation describes the viscous energy losses and the third term the kinetic energy losses. This became known as the Ergun equation, and it is valid in the range of $1 < Re_p < 2500$ and $0.36 < \epsilon < 0.4$. Ergun (1952) believed that the wall effect had a negligible impact on the pressure drop over a packed bed, therefore the Ergun equation does not take the wall effect into account (Erdim, et al., 2015). Later researchers modified the parameters a and b in Eq. (2.9) to better account for the viscous and kinetic energy losses at low and high flow rates, respectively.

Hicks (1970) noted that the Ergun equation was only valid for $Re_m < 500$, which severely limited the applicability of the correlation. Hicks (1970) went on to develop a substitute expression which was applicable for $\frac{Re}{1-\epsilon} > 300$ (Hicks, 1970):

$$\frac{\Delta P}{L} = 6.8 \cdot \frac{(1-\epsilon)^{1.2}}{Re^{0.2}\epsilon^3} \tag{2.10}$$

On the contrary, Tallmadge (1970) asserted that the Ergun equation is valid for flows of $Re_m < 1000$, and attempted to extend the equation to higher Reynolds numbers (up to $Re_m < 10^5$), by modifying the coefficient b and the exponent n in the Ergun equation (Eq. 2.6). Tallmadge (1970) analytically determined these coefficients by studying the data of Wentz and Thodos (1963) due to the large number of data points available which covered a wide range of Reynolds numbers, and proposed Eq. (2.11):

$$\frac{\Delta P}{L} = \frac{150}{Re_m} + \frac{4.2}{Re_m^{\frac{1}{6}}} \tag{2.11}$$

Mehta and Hawley (1969) were the first to attempt to account for the wall effect, by modifying the Ergun equation to consider the effect of the confining walls on the hydraulic radius (Eq. 2.12):

$$\frac{\Delta P}{L} = 150 \cdot \frac{(1-\epsilon)^2}{\epsilon^3} UM^2 + 1.75 \cdot \frac{1-\epsilon}{\epsilon^3} \rho U^2 M \tag{2.12}$$

Where

$$M = 1 + \frac{4d_p}{6D(1-\epsilon)} \tag{2.12a}$$

Eisfeld and Schnitzlein (2001) also modified the Ergun equation to better consider the wall effect on the pressure drop over a packed bed. Their equation introduces two coefficients: M and B_w, where M is the same as given by Mehta and Hawley (1969), and B_w describes the porosity change at the walls:

$$\Psi = \frac{154M^2}{Re_p} \cdot \frac{(1-\epsilon)^2}{\epsilon^3} + \frac{M}{B_w} \cdot \frac{1-\epsilon}{\epsilon^3} \tag{2.13}$$

Where the coefficients M and B_w are given by:

$$M = 1 + \frac{2}{3\left(\frac{D}{d_p}\right)(1-\epsilon)} \tag{2.13a}$$

And

$$B_w = \left[1.15\left(\frac{d_p}{D}\right)^2 + 0.87\right]^2 \tag{2.13b}$$

Di Felice and Gibilaro (2004) suggested a two-zone flow model to account for both the bypass effect and wall friction at all flow regimes. In this model, the bed was separated into two distinct regions: the wall and bulk zone. They proposed that the bulk porosity be used in the Ergun equations. The bulk porosity, ϵ_B, is the porosity of the bed one sphere diameter from the wall in the radial direction. The bulk fluid flux, ϕ_B, is calculated from Eq. (2.14):

$$\Phi_B = \frac{\Phi}{2.06 - 1.06\left(\alpha - \frac{1}{\alpha}\right)^2} = \frac{Q}{A(2.06 - 1.06\left(\alpha - \frac{1}{\alpha}\right)^2} \tag{2.14}$$

Where Φ is the average fluid flux, Q is the average volumetric flowrate and A is the flow cross-section. This therefore circumvents the uncertainties caused by the wall effect by only considering the flow in the bulk region (Di Felice & Gibilaro, 2004).

Wentz and Thodos (1963) performed pressure drop experiments for both packed and distended beds of mono-sized spherical particles for modified Reynolds numbers $2550 \leq Re_m \leq 64900$, and developed a correlation to predict the friction factor, and by extension the pressure drop:

$$\Psi = \frac{0.792}{Re_m^{0.05} - 1.2} \tag{2.15}$$

The German Nuclear Safety Standard Commission (KTA, 1981) attempted to determine a correlation for the friction factor of a fluid flowing through a packed pebble bed. This correlation was intended to give accurate predictions over a large range of Reynolds numbers, and it was derived from various correlations available in literature. The correlation was obtained by studying experimental data from various studies. For the data to be considered viable, the experiment it was obtained from had to comply with the following criteria:

- The effect of the confining wall had to be minimal.
- The average porosity had to be noted.

- The length to particle diameter ratios $\frac{L}{d_p}$ of all beds had to be larger than 4.
- Randomly packed beds had to be used to develop the correlations.
- The spheres had to have a diameter larger than 1 mm.

The KTA proposed correlations for the pressure drop (Eq. (2.14)) and friction factor (Eq. (2.15)) over a packed bed which were derived from the studied experimental data (KTA, 1981):

$$\Delta P = \left(\frac{320}{Re_m} + \frac{6}{Re_m^{0.1}}\right) \cdot \mathrm{L} \cdot \frac{1-\epsilon}{\epsilon^3} \cdot \frac{1}{d_p} \cdot \frac{1}{2\rho} \cdot U^2 \tag{2.14}$$

And

$$\Psi = \frac{320}{Re_m} + \frac{6}{Re_m^{0.1}} \tag{2.15}$$

The KTA correlations are valid for packed beds with cylindrical cross-sections which consist of mono-sized spheres, which have the following flow and structural parameters:

- $1 < Re_m < 10^5$.
- $0.36 < \epsilon < 0.42$.
- $L > 5d_p$.
- The aspect ratio of the beds had to be chosen according to the following limiting curve in Figure 2.3-1:

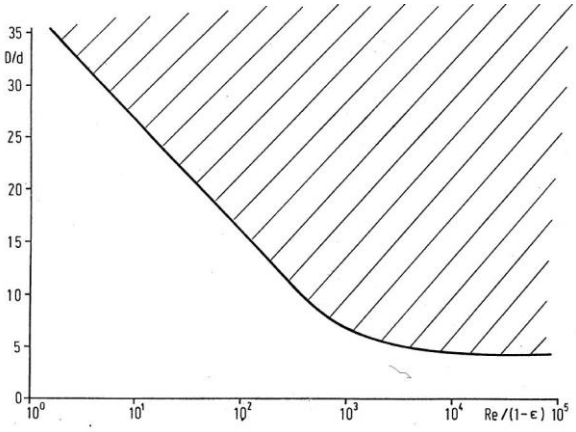

Figure 2.3-1: Limiting curve of the aspect ratio as a function of the modified Reynolds number (KTA, 1981)

Figure 2.3-1 shows the limiting curve of the aspect ratios as functions of the modified Reynolds number. The shaded area represents the aspect ratios for which the KTA friction factor is valid for at specific modified Reynolds numbers. It is apparent that for the higher Reynolds numbers, the KTA cannot predict the pressure drop over beds with aspect ratios above 5, reducing the applicability of the correlation. It should also be noted that the KTA friction factor correlation does not consider the influence of the wall effect on the pressure drop through a packed bed.

2.4 CFD Modelling of the flow through a packed bed

Computational Fluid Dynamics (CFD) is the method of using computers to simulate flow systems (Versteeg & Malalasekera, 2007). With the aid of CFD, it is possible to accurately simulate and analyse complex flow and heat transfer properties without resorting to expensive and time-consuming physical experiments. Several papers have been published that prove the validity of CFD simulations of packed beds, due to results obtained from these simulations being in close agreement to physical experiments (Calis, et al., 2001).

The purpose of this subsection is to gain insight from previous authors into CFD modelling of flow through packed beds to ensure the simulations of this study are representative of actual flow conditions.

2.4.1 Mesh generation

Numerical three-dimensional CFD solvers require that a geometry should be discretized by means of a volume mesh through which a solution for the flow problem can be generated using an iterative process (Versteeg & Malalasekera, 2007). Volume meshes can be generated using, amongst others, two types of cells: tetrahedral and polyhedral cells. Tetrahedral cells consists of tetrahedrons (triangular volumes with four faces), which means that each cell is surrounded by four other cells, whilst polyhedral cells can assume any geometric shape and can have up to ten neighbouring cells (Peric & Ferguson, 2008); and both types of meshes have been used to simulate flow through packed beds. The quality of the volume mesh greatly effects various aspects of the simulation, such as the stability, accuracy, ability to convergence and convergence rate (CD-Adapco, 2012).

The complexity of the packed bed, specifically the points where contact occurs between adjacent spheres and where spheres contact the containing walls; increases the difficulty to generate high-quality meshes. Several attempts have been made to address these issues in the mesh generation for packed beds (Baker & Tabor, 2010).

Calis et al. (2001) generated unstructured tetrahedral meshes over the packed beds. The hurdle that contact points represented was overcome by simply eliminating them. It was found that the contact points could be eliminated by reducing the sphere diameters by one percent after mesh generation, which creates gaps between the spheres, improving the mesh quality (Calis, et al., 2001). The mesh quality was also improved by adding prismatic cells near the wall regions, which created a so-called prism layer. This also had the added effect of resolving the viscous flow near the walls. It was found that a reduction in the thickness of the prism layer was necessary when simulating turbulent flows, and it was also found that by refining the mesh over the spheres also improved the mesh quality considerably (Calis, et al., 2001).

A similar approach to Calis et al. (2001) was used by Reddy and Joshi (2008), who also used tetrahedral meshes and shrunk the spheres to eliminate the contact points to generate a high-quality mesh (Reddy & Joshi, 2008). Analysis of the fluid flow in the gaps between the spheres revealed that the fluid had a velocity that was close to zero in these areas. This led them to conclude that the gaps between the spheres had no impact on the flow pattern through the bed (Reddy & Joshi, 2008).

Eppinger et al. (2011) also attempted to improve the mesh quality by addressing the contact points. Using a polyhedral mesh, a method was developed which flattens the cells in the contact region if the minimum distance between the two spheres drop below a specified value, creating a gap between the spheres without changing their respective diameters. It was further noted that by extending the inlet by three particle diameters and the outlet by ten particle diameters from the bed respectively, the influence that the boundary conditions at these regions has on the packed bed region could be eliminated (Eppinger, et al., 2011).

Van der Merwe (2014) was able to generate a high-quality mesh for a cylindrical packed bed using polyhedral cells and by adapting the contact points. The contact points were adapted by creating a fillet with a small radius at all contact points as shown in Figure 2.4-1:

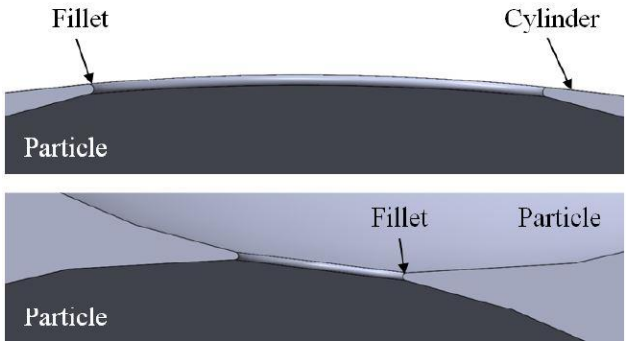

Figure 2.4-1: Elimination of contact points by using fillets (Van der Merwe, 2014)

As suggested by Calis et al. (2001), the mesh over the spheres was much finer than the global settings (10% the size of the global mesh). During a mesh dependence study, Van der Merwe (2014) found that a mesh which consists of polyhedral cells, with a base size of 3 mm, with two prism layers over the spheres and near the walls, with a finer mesh over the spheres, and that has had the contact points adapted by using fillets, generated a high-quality mesh with relatively few skewed cells (0.017% of the total number of cells) and degenerate cells (0.0155% of the total number of cells).

Lopes and Quinta-Ferreira (2008) tested both a fine global mesh and a mesh which was coarse globally but was locally refined over the packed bed. It was found that the there was no difference between the hydrodynamic properties of a fine global mesh and a locally refined mesh. However, fewer cells are generated with the locally refined mesh, which means that the strain that was placed on the solver was reduced significantly (Lopes & Quinta-Ferreira, 2008).

Preller (2011) attempted to generate a high-quality mesh over a considerably more complex packed bed, that of the Braiding Effects Test Section of the PDTS experiments. A thin mesh was used in conjunction with a higher surface growth rate (1.5 versus the default 1.2) with no prism layers, that had a base size of 3.5 mm. This mesh consisted of 15.4 million polyhedral cells, but more than 52% of the cells had a quality of less than 50% (Preller, 2011).

Vermaak (2019) attempted to improve on the mesh generated by Preller (2011). Vermaak (2019) slightly increased the base size of the mesh (4 mm) and decreased the surface growth rate (1.3 vs 1.5). The polyhedral mesh density and growth factor were increased (1 vs. 1.2) and reduced (1 vs. 0.85) respectively, relative to the mesh settings used by Preller (2011). Two prism layers were also added that were 17.5% the thickness of the base size. The mesh generated had a reduced number of cells (9.7 million), and the number of cells with a quality less than 50% was reduced by over 50% compared to the mesh generated by Preller (2011) (Vermaak, 2019).

2.4.2 Turbulence models

In CFD simulations, several turbulence models are available, and the turbulence model can greatly influence the simulation accuracy, stability and ability to converge. Several turbulence models are available which solve the turbulence in different manners. Large Eddy Simulations (LES) and Reynolds-Averaged Navier-Stokes (RANS) models are two of the main models used in CFD simulations. Several authors have tested the accuracy of these models for pressure drop over a packed bed (Calis et al. (2001), Hassan (2008), Vermaak (2019)).

Calis et al. (2001) analysed the pressure drop over a packed bed with an aspect ratio of between 1 and 2 using CFD. The difference in accuracy between the Reynolds Stress Model (RSM) and the $k-\epsilon$ turbulence model was investigated, and it was found that there was only a small difference in the pressure drop between the two models (less than 10% error percentage). This means that the $k-\epsilon$ model is preferable to the RSM model due to the increase in computational demand of the RSM model (Calis, et al., 2001).

The difference in accuracy of the pressure drop predictions of the various RANS turbulence models was also investigated by Bai et al. (2009). The turbulence models in question were the $k-\epsilon$, $k-\omega$ and RSM models. The pressure drop over the packed bed from the simulations was compared with experimental results. It was found that the pressure drop values predicted by the RSM model were the most accurate, coming to within 3% of the experimental values, and that the $k-\epsilon$ and $k-\omega$ turbulence models showed little difference in terms of the predicted pressure drop (less than 4% difference), whilst still predicting pressure drops close to those predicted by the RSM model (less than 3% difference). Again, it was found that the additional computational resources required by the RSM model were not justified (Bai, et al., 2009).

Hassan (2008) compared the accuracy of LES and RANS models. The LES used the Smogarinsky subgrid-scale (SGS) and $k-\epsilon$ model was the chosen RANS model. During testing it was found that LES predicted a pressure drop that was more accurate than that predicted by the $k-\epsilon$ model; however, a much finer mesh was required, which increased the solution time (Hassan, 2008).

Van der Merwe (2014) also investigated the difference in accuracy between LES and $k-\epsilon$ turbulence models. The pressure drop was determined for particle Reynolds numbers of $Re_p = 1000$ and $Re_p = 10000$. The LES, being an inherently transient model, was run for 30 seconds in the former case and for 3 seconds for the latter case. The $k-\epsilon$ model was tested for steady state. Both turbulence models used fully developed flow velocity profiles at the inlet. It was found that the difference between the predicted pressure drop between LES and $k-\epsilon$ at $Re_p = 1000$ was 0.77%, and at $Re_p = 10000$ the difference between them was 1.01%. Therefore, it was decided to use the $k-\epsilon$ model due to it requiring fewer computational resources than the LES turbulence model (Van der Merwe, 2014).

2.4.3 Pressure drop prediction accuracy

Several authors have compared the pressure drop predicted by CFD simulations to practical experimental results and found that the results are usually in good agreement with each other

(Reddy & Joshi (2008), Bai et al. (2009), Eppinger et al. (2010)). Due to the high accuracy of the simulations, it is possible to analyse the effect of various parameters on the pressure drop over the packed bed.

Bai et al. (2009) compared the CFD modelling of the pressure drop over a structured packed bed with experimental results. The CFD generated beds were exact replicas of the experimental setup. It was found that the CFD simulations predicted pressure drops that on average were 3.1% lower than the experimental results. This discrepancy was traced to the geometry, specifically the spheres, whose diameters were reduced by 0.5% to remove the effect of the contact points. When a correction factor was introduced to correct for this effect, the error between the simulated and experimental results was reduced to 2% (Bai, et al., 2009).

Baker and Tabor (2010) simulated the flow over a randomly packed bed consisting of 160 spheres with an aspect ratio of 7.14, over a wide range of particle Reynolds numbers ($700 \leq Re_p \leq 5000$). A bed with similar structural parameters was built to physically test the pressure drop. It was found that the experimental results compared well with the correlation for the friction factor proposed by Eisfeld and Schnitzlein (2001). The pressure drop predicted by the simulation also compared well with the experimental results and to those predicted by the Eisfeld and Schnitzlein (2001) correlation. This suggests that CFD simulations can mimic the effect of the containing wall on the flow and pressure drop of the fluid (Baker & Tabor, 2010).

Eppinger et al. (2011) analysed the pressure drop over beds with aspect ratios varying from 3 to 10, in the laminar, transitional and turbulent flow regimes, and compared the results with those available in literature. It was found that the maximum deviation in the pressure drop values predicted by the CFD simulation from those calculated from the Eisfeld and Schnitzlein (2001) correlation was 15%, which occurred once in the laminar as well as in the turbulent flow regimes, respectively. This further confirms that CFD can be used to predict the effect that the containing wall has on the pressure drop with a high degree of accuracy (Eppinger, et al., 2011).

Atmakadis and Kenig (2009) used a CFD-based analysis to model the pressure drop through four structured packed beds in the laminar flow regime. Two of these beds had a body-centred cubic structure, with aspect ratios of 1 and 2.68, respectively; and the other two had a face-centred cubic structure with aspect ratios of 3 and 5.5, respectively. During testing, it was found that the pressure drop over the structured beds compared the best with the correlation proposed by Susskind and Becker (1967), which takes the wall effect into account (Atmakidis & Kenig, 2009). It was also observed that in the wall region, high local velocities of the fluid were possible due to the increase in the porosity in these regions (Vollmari, et al., 2015).

Similarly, Reddy and Joshi (2010) also used a CFD-based approach to simulate the wall effect on the pressure drop. They used three random packed beds, with cylinder-to-particle ratios of 3, 5 and 10 to simulate the pressure drop over the bed in the viscous, transitional and turbulent flow regimes. Reddy and Joshi (2010) found that the friction factor was higher than that predicted by the Ergun equation in the creeping flow regime, which was caused by increased wall friction. Conversely, the friction factor was lower than that predicted by the Ergun equation in the turbulent regime, which was due to increased velocity caused by the bypass effect (Reddy & Joshi, 2010).

2.5 Summary

The aim of this literature survey was to gain insight into the influence that various parameters, structural and otherwise, have on the pressure drop over random and structured packed beds consisting of mono-sized spherical particles; as well as to understand the methods and correlations which have been proposed to predict the pressure drop. The structural parameters that were found to influence the pressure drop over a structured packed bed are the aspect ratio, porosity, particle size, structuredness and the wall effect.

It was found that an increase in the aspect ratio, the ratio of the container diameter to the particle diameter, led to an increase in the pressure gradient over a packed bed. However, the very definition of the aspect ratio can only be applied to cylindrical beds of mono-sized spherical particles.

The porosity was found to have a pronounced effect on the pressure drop over a packed bed. An increase in the porosity of the bed led to a decrease in the pressure drop over the bed, even when the bed had the same packing structure and was tested for the same flow conditions as the lower porosity bed. Additionally, the pressure drop over the bed became much more sensitive to an increase in porosity for higher porosities, as can be seen in Figure 2.1-3, and also being more sensitive under turbulent flow conditions than in laminar flow conditions.

The influence that the particle size had on the pressure drop over the packed bed was found to be significant. Beds consisting of particles of smaller diameters experienced a higher pressure drop over the bed than those of consisting of particles of larger diameters, as can be seen in Figure 2.1-6 to Figure 2.1-8.

Whether the bed was structured or unstructured (randomly packed) also significantly influenced the pressure drop. The pressure drop through a random packed bed was greater than the pressure drop through a structured bed. The specific structure of the bed is also of importance when considering the pressure drop – for instance, a bed with a SC structure will have a lower

pressure drop over the bed than a bed with a FCC structure, even when the aspect ratios, porosities, particle sizes and flow conditions were very similar. Furthermore, the lateral spacing between the spheres also greatly influenced the pressure drop over the bed, with a larger spacing leading to an increase in the channelling effect, causing the pressure drop over the packed bed to decrease.

The effect that the containing wall has on the pressure drop over a packed bed was also investigated, and its effects were found to be largely dependent on the Reynolds number of the flow. Finite packed beds, whether structured or unstructured, experience an increase in porosity due to the containing walls, which causes a bypass effect. The containing walls also lead to an increase in viscous energy losses, due to the friction of the fluid flowing past the wall. At low Reynolds numbers, the wall friction is dominant, leading to an increase in the friction factor of the packed bed. At high Reynolds numbers, the bypass effect is dominant, increasing the local fluid velocity, leading to a reduction in the friction factor of the packed beds.

Various semi-empirical pressure drop prediction correlations have been proposed which were derived from experimental or theoretical studies. These correlations were found to be accurate only under very specific structural and flow conditions. Many of these correlations did not consider the effect that the containing wall has on the pressure drop, and several authors have proposed corrections to these predictions to compensate for it. Currently, no clear consensus has been reached on which correlations can be universally used to describe the pressure drop of a fluid flowing through a packed bed; regardless of structural or flow parameters.

Previous studies to model the pressure drop over a packed bed using a CFD-based analysis were also investigated. It was found that a sufficient quality mesh is of great importance, as it can influence the simulation accuracy, convergence rate and stability. High quality meshes can be generated using polyhedral cells with a specific number of prism layers, which have the added benefit of resolving the viscous sublayer as the fluid moves over the spheres. A mesh that is refined locally over the spheres captures the flow properties over the bed much better but requires more resources. It was found that the $k-\epsilon$ turbulence model delivers results which are in close agreement to Large Eddy Simulations and $k-\omega$ results. However, LES requires a much finer grid and more resources to generate high accuracy results, and $k-\epsilon$ models can not solve the viscous sublayer specifically. From the literature, it is apparent that CFD is able to accurately predict the pressure drop over a packed bed, including the effect that the containing wall has on the pressure drop.

CHAPTER 3: METHODOLOGY

In this chapter, a brief theoretical background of Computational Fluid Dynamics will be discussed, as well as the methodologies used for the Wentz and Thodos (1963) mesh dependence study and PDTS simulations.

3.1 Methodology: Theoretical Background

3.1.1 Computational Fluid Dynamics

Computational Fluid Dynamics (CFD) is the method of using computers to numerically solve and simulate systems of fluid flow, heat transfer and various other phenomena. The simulation of fluid flow phenomena requires governing equations which mathematically represent the laws of conservation of physics. These laws are as follow (Versteeg & Malalasekera, 2007):

1. The fluid mass is conserved;
2. The sum of forces acting on a particle equals the rate of change of momentum of the particle; and
3. The sum of the rate of heat addition to, and the rate of work done on, a fluid particle is equal to rate of change of energy of the particle.

In this section, the discretization and application of the equations which are based on the above-mentioned laws to a finite number of control volumes will be discussed briefly.

3.1.1.1 Transport equations

Continuum fluid mechanics can be described by conservative fluid flow equations. These equations are conservative because it is assumed that the mass, entropy, momentum and energy of the fluid are conserved. If a variable ϕ is chosen to represent a flow property, its transport equation can be written as in Eq. (3.1):

$$\frac{\partial \rho \phi}{\partial t} + \nabla(\rho \phi \boldsymbol{u}) = \nabla(\Gamma \nabla \phi) + S_\phi \tag{3.1}$$

The first term in Eq. (3.1) denotes the rate of change in ϕ, the second term the convective term ($\boldsymbol{u}$ is the vector velocity field), the third term is the diffusion term (where Γ is the diffusion coefficient), and the fourth term is the source term.

By setting $\phi = 1$, $\phi_x = u$, $\phi_y = v$, $\phi_z = w$ and $\phi = i$ respectively; and by choosing suitable values for Γ an S_ϕ, Eq. (3.1) is transformed into the system of equations governing the three-dimensional time-dependent heat transfer and fluid flow of a fluid (Versteeg & Malalasekera, 2007):

$$\frac{\partial \rho}{\partial t} + \nabla(\rho \boldsymbol{u}) = 0 \tag{3.2}$$

$$\frac{\partial \rho u}{\partial t} + \nabla(\rho u \boldsymbol{u}) = -\left(\frac{\partial p}{\partial x}\right) + \nabla(\mu \nabla u) + S_{Mx} \tag{3.3}$$

$$\frac{\partial \rho v}{\partial t} + \nabla(\rho v \boldsymbol{u}) = -\left(\frac{\partial p}{\partial y}\right) + \nabla(\mu \nabla v) + S_{My} \tag{3.4}$$

$$\frac{\partial \rho w}{\partial t} + \nabla(\rho w \boldsymbol{u}) = -\left(\frac{\partial p}{\partial z}\right) + \nabla(\mu \nabla w) + S_{Mz} \tag{3.5}$$

$$\frac{\partial \rho \upsilon}{\partial t} + \nabla(\rho i \boldsymbol{u}) = -p \nabla \boldsymbol{u} + \nabla(\kappa \nabla T) + \Omega + S_i \tag{3.6}$$

$$p = p(\rho, T) \tag{3.7}$$

$$i = i(\rho, T) \tag{3.8}$$

Where $p = p(\rho, T)$ and $i = i(\rho, T)$, are the fluid pressure and specific internal energy respectively, as functions of density and temperature. Equation (3.2) is the continuity equation. Equations (3.3) to (3.5) are the momentum equations in the x, y, and z directions respectively. Equation (3.6) is the energy equation, with i the specific internal energy, κ the thermal conductivity coefficient and Ω a dissipation function (Versteeg & Malalasekera, 2007).

3.1.1.2 Finite volume method

The application of the governing conservation equations to a solution domain requires that the domain must first be discretized into control volumes, each one corresponding to a cell in a computational grid (Versteeg & Malalasekera, 2007). Firstly, Eq. (3.1) is integrated over a control volume:

$$\int \frac{\partial \rho \phi}{\partial t} dV + \int \nabla(\rho \phi \boldsymbol{u})\, dV = \int \nabla(\Gamma \nabla \phi) dV + \int S_\phi \, dV \tag{3.9}$$

Where dV denotes an infinitesimal volume of the control volume. If the flow is considered steady-state, then the first term of equation (3.9) becomes zero. Eq. (3.9) can be further transformed by the application of Gauss' Divergence Theorem to the second and third terms in the equation, which transforms it into Eq. (3.10):

$$\int \frac{\partial \rho \phi}{\partial t} dV + \int (\rho \phi \boldsymbol{u}) \cdot dS = \int (\Gamma \nabla \phi) \cdot \mathrm{dS} + \int S_\phi \, \mathrm{dV} \tag{3.10}$$

Where dS is the surface vector on the boundary of the control volume, pointing outwards from the control volume.

3.1.1.3 Solver models

Two approaches are available to solve the flow of a fluid in Star-CCM+: segregated and coupled flow solvers. These two solvers will be discussed briefly.

3.1.1.3.1 Segregated Flow Solver

The Segregated Flow Solver model solves the momentum and mass conservation equations separately, with the non-linear governing equations in Section 3.1.1.1 being solved iteratively for the variables in Eqs. (3.3) – (3.8). The pressure and velocity of the fluid are coupled with an algorithm which seeks to fulfil the mass conservation equation on the velocity field, which is achieved by solving a pressure-correction equation, which in turn originates from the momentum and continuity equations that predict a velocity field that satisfies the continuity equation by correcting the pressure. Thus, the Segregated Flow Solver uses a prediction-correction approach and uses two algorithms to couple pressure and velocity: SIMPLE and PISO (CD-Adapco, 2012).

The Segregated Flow Solver employs a Gauss-Seidel type iterative solving technique. The Segregated Flow Solver model achieves convergence faster than the Coupled Flow Solver model, while using less memory (CD-Adapco, 2012).

3.1.1.3.2 Coupled Flow Solver

The Coupled Flow Solver model solves the equations for momentum and mass conservation, as well as for energy, simultaneously as a vector of equations. The velocity field is calculated from the momentum equations, and the density and pressure is calculated from the equation of state. The Coupled Flow Solver can be used to model the flow of a fluid in both steady and unsteady states, and it is able to achieve convergence whether a fine or coarse mesh is used (CD-Adapco, 2012).

3.1.1.4 Energy models

3.1.1.4.1 Segregated fluid isothermal

With the Segregated Fluid Isothermal model, the temperature in the continuum is kept constant. This energy model is used where the temperature variations in the fluid are negligible, since to solve the energy transport equation for essentially a constant temperature field would be too computationally expensive (CD-Adapco, 2012).

3.1.1.4.2 Segregated fluid temperature

With the Segregated fluid temperature model, the energy equation is solved independently from the other conservation equations by using the temperature as an independent variable. The equations of state are then used to obtain the temperature as part of an iterative sequence in the segregated flow solver (CD-Adapco, 2012).

3.1.1.4.3 Coupled energy

The Coupled Energy model is a built-in extension of the Coupled Flow Solver. The Coupled Energy models solves the equations for the conservation of energy, momentum and mass simultaneously in conjunction with the Coupled Flow Solver (CD-Adapco, 2012).

3.1.1.5 Turbulence

Two categories of turbulence models can be used in Star-CCM+: Reynolds-Average Navier-Stokes (RANS) turbulence, and Scale-Resolving Simulations. These two categories will be discussed briefly in this section (CD-Adapco, 2012).

3.1.1.5.1 Reynolds-Averaged Navier-Stokes Turbulence

The Reynolds-Averaged Navier-Stokes (RANS) equations are formed by time-averaging Eq. (3.1), and Eqs. (3.3) to (3.7) and decomposing them into an average and fluctuating component, respectively. These equations therefore remain essentially the same, with the addition of a stress tensor quantity, $\boldsymbol{T_t}$. This stress tensor is defined as given in Eq. (3.11):

$$\boldsymbol{T_t} = -\rho \begin{bmatrix} \overline{u'u'} & \overline{u'v'} & \overline{u'w'} \\ \overline{u'v'} & \overline{v'v'} & \overline{v'w'} \\ \overline{u'w'} & \overline{v'w'} & \overline{w'w'} \end{bmatrix} \tag{3.11}$$

The RANS turbulence model models $\boldsymbol{T_t}$ in terms of mean flow quantities to satisfy the governing equations mentioned in Section 3.1.1.1. One of the methods used to satisfy the governing equation is the Eddy Viscosity Model. The Eddy Viscosity Model solves further transport equations for scalar quantities that give rise to the turbulent viscosity, μ_t (CD-Adapco, 2012). The turbulent viscosity make it possible to model the stress quantity as a function of mean flow qualities with various turbulence models. Two of these models and their variants, k-epsilon ($k-\epsilon$) and k-omega ($k-\omega$), will be discussed briefly.

$k-\epsilon$ models

The $k-\epsilon$ model is a two-equation model that calculates μ_t by solving the transport equations for the turbulent kinetic energy k and turbulent dissipation rate ϵ [(Versteeg & Malalasekera, 2007), (CD-Adapco, 2012)].

$k-\omega$ models

The $k-\omega$ turbulence model is also a two-equation model, which also solves the transport equation equations to determine the turbulent viscosity. However, the transport equations are solved for the turbulent kinetic energy, k and the specific dissipation rate ω – the dissipation rate per unit turbulent kinetic energy [(Versteeg & Malalasekera, 2007), (CD-Adapco, 2012)].

3.1.1.5.2 Scale-Resolving Simulations

Scale-resolving simulations resolve the large scales of turbulence and model the small-scale motions. The most popular Scale-Resolving Simulation used is the Large Eddy Simulation, or LES.

Large Eddy Simulation

LES is an inherently transient method of simulation. The LES model solves turbulence everywhere in the volume to the grid limit, where the impact of the sub-grid structures on the flow field is approximated by sub-grid models – typically the Smogarinsky or WALE (Wall-Adapting Local-Eddy) sub-grid scale models (Versteeg & Malalasekera, 2007).

3.1.1.6 Wall treatment

It is necessary to be able to accurately predict flow and turbulence parameters over the boundary wall layer, since the walls act as the origin of vorticity in fluid flow. The boundary layer can be differentiated into three distinct sublayers: the viscous, log-law and buffer layers. The flow of the fluid in each layer has different characteristics. In the viscous sublayer, viscous effects dominate over the fluid layer, which is in contact with the wall, with the flow velocity being dependent on the fluid viscosity, density, wall shear stress and the physical distance from the wall. The buffer layer act as the intermediate layer between the viscous and log-law layers. In the log-law layer, both turbulent and viscous effects are equally dominant over the fluid flow (CD-Adapco, 2012).

The wall distance y^+, a non-dimensional value, can be used to define the extents of the sublayers, and is defined as in Eq. (3.12):

$$y^+ = \frac{yu^*}{v} \tag{3.12}$$

In Eq. (3.12), y is the distance from the wall to the specific centroid of the applicable control volume, u^* is the reference velocity, and v is the kinematic viscosity.

Star-CCM+ has three wall treatments that can be applied to a simulation:

- Low-y^+ wall treatment: this wall treatment resolves the viscous sublayer and the flow across the wall boundary is predicted with little modelling. The transport equations are solved all the way down to the wall cell. The shear stress of the fluid due to its proximity to the wall is calculated in the same manner as laminar flow. An adequately fine mesh with cells located at y^+ values close to one is required to resolve the viscous layer. The viscous sublayer can become thin for high Reynolds number flows, so this wall treatment is usually selected when low-Reynolds number flows are being simulated (CD-Adapco, 2012).
- High-y^+ wall treatment: this wall treatment obtains boundary conditions for the continuum equations from wall functions and does not resolve the viscous sublayer, and it is assumed that the cells which are located next to the wall are within the log-law flow sub-layer. Turbulent production and dissipation, as well as wall shear stress are obtained from the boundary layer theory for equilibrium turbulence (CD-Adapco, 2012).
- All-y^+ wall treatment: this wall treatment imitates the low-y^+ treatment for fine meshes as well as the high-y^+ wall treatment used with coarse meshes. Turbulent quantities such as production, stress tensor and dissipation are calculated with a blending function (CD-Adapco, 2012).

Some Reynolds-Averaged Navier-Stokes turbulence models or model variants cannot be used with certain wall treatments, due to the model not resolving the turbulence in the viscous sublayer. With Large Eddy Simulations, it is insufficient to merely stretch the mesh only normal to the wall, making the resolution of the viscous sublayer potentially computationally expensive (CD-Adapco, 2012).

3.1.1.7 Mesh generation

The mesh density and quality has a serious impact on solution accuracy and stability, making the generation of a satisfactory mesh an important part of CFD simulations. The volume mesh mathematically describes the domain of the simulation which will be solved. In Star-CCM+, the

volume mesh is started from the surface mesh, and is constructed from the following entities (CD-Adapco, 2012):

- Vertices – points in space that can be specified by a position vector.
- Faces – surfaces in three-dimensional space that are defined by an ordered collection of vertices
- Cells – a closed volume defined by an ordered collection of faces.

The mesh continua contain various mesh parameters, such as the following:

- Base size – a dimensional definition of the geometry of the simulation being solved, which defines the desired surface cell length. All other mesh properties are usually set in relation to the base size.
- Surface sizes – the size of the cells next to the domain surfaces are determined according to the values set for the surface size. The surface size is normally set with a minimum and target size – which define the lower limit of the edge cell length and the preferred edge cell length on the surface, respectively.
- Surface growth rate – the rate at which the edge lengths of the cells can change from one cell to the next is controlled by this parameter. This is a useful parameter for the local refinement of a volume mesh.
- Prism layer thickness – defines the desired thickness of the orthogonal prismatic cells next to surfaces.

Unstable or inaccurate solutions can often be traced to too coarse meshes. On the contrary, meshes that are too fine will require more computational resources (CD-Adapco, 2012). Therefore, using a mesh which gives a good compromise between result accuracy and resources (time and computational) is of great importance in Computational Fluid Dynamics simulations (Lopes & Quinta-Ferreira, 2008).

3.2 CFD Simulation Methodology – Wentz and Thodos (1963) simulations

This section will discuss the details of the CFD simulation methodology which was used to validate the experiments of Wentz and Thodos (1963) of the pressure drop of a fluid flowing through a packed bed of porosity $\epsilon = 0.354$, and to conduct the mesh dependence study. The default physics and mesh continua values in Star-CCM+ version 12.02.011 were used unless otherwise stated. This methodology is based on the methodology used by Van der Merwe (2014), with some changes made to the physics continua and stopping criteria.

3.2.1 Geometry

Star-CCM+ requires the geometry of the computational domains to create a mesh for the numerical solver. The domains were created using the CAD program SolidWorks (2016) and were created by Van der Merwe (2014). The geometry consists of solid spheres repeated with linear patterns to complete the BCC structure, surrounded by a cylinder; which reflects the experimental setup used by Wentz and Thodos (1963), as shown in Figure 3.2-1:

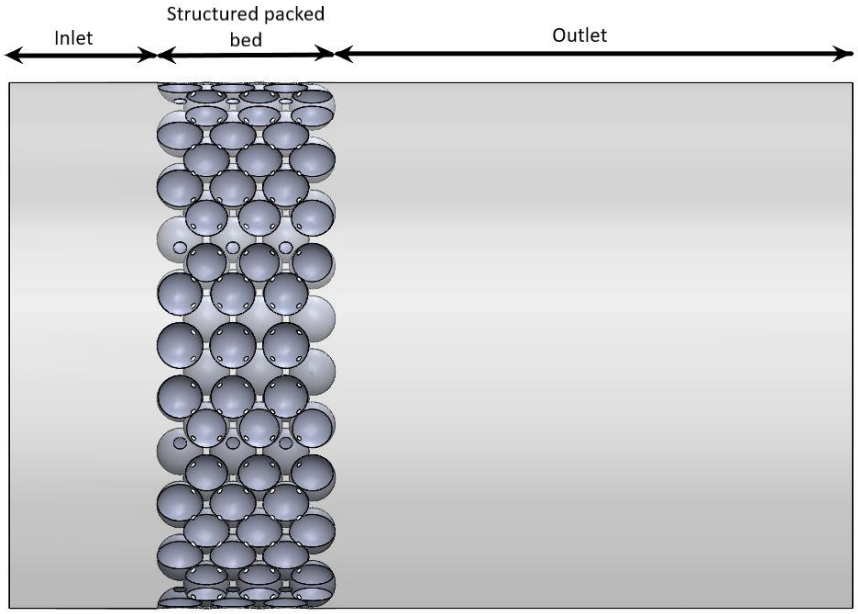

Figure 3.2-1: Geometry used to simulate the Wentz and Thodos (1963) experiment

Van der Merwe (2014) generated a bed that had a porosity of $\epsilon = 0.383$, compared to a porosity of $\epsilon = 0.354$ that was reported by Wentz and Thodos (1963). The domains were split into four regions: the inlet, structured packed bed, outlet and cylinder regions as described by Van der Merwe (2014). In accordance with the findings of Eppinger et al. (2011), the inlet was extended by 100 mm (more than three particle diameters) and the outlet by 350 mm (more than ten particle diameters) to eliminate the effects of the boundaries on the flow through the packed bed region.

3.2.2 Boundaries

As previously mentioned, the domains in Star-CCM+ were divided into four distinct regions with boundary conditions specified as in Table 3.2-1:

Table 3.2-1: Regions of the Wentz and Thodos (1963) simulation domains and their respective boundary conditions

Region	Boundary condition
Inlet	Velocity inlet
Pebbles	No-slip wall
Cylinder	No-slip wall
Outlet	Pressure outlet

The control volume was modelled adiabatically, therefore no heat transfer over any boundaries was modelled. An ambient temperature and pressure of 300 K and $p_a = 101.325\,kPa$, respectively were used for all simulations (Van der Merwe, 2014).

3.2.3 Mesh continua

The mesh continua were based on the findings of Van der Merwe (2014), and the following meshing models were chosen for all the meshing models:

- Surface remesher
- Polyhedral volume mesher
- Prism layer mesher

All volume meshes were tessellated with a fine tessellation density. Table 3.2-2 gives the values of some of the parameters that were specified when generating the mesh for the Wentz and Thodos (1963) simulations (Van der Merwe, 2014):

Table 3.2-2: Wentz and Thodos (1963) simulation mesh parameters

Parameter	Value
Base size, B	Varies
Minimum surface size	$0.25B$
Target surface size	$1.00B$
Number of prism layers	2
Prism layer thickness	$0.2B$

3.2.4 Physics continua

For the mesh dependence study, the physics continua were kept the same for all simulations. The physics continua were chosen according to the best practices suggested by CD-Adapco (2012), and were chosen as follows:

- Steady
- Ideal gas: air
- Compressible flow
- Turbulent
    - Realizable $k-\epsilon$ turbulence model
    - Two-layer all y^+ wall treatment

The flow and energy models used for all simulations were segregated and coupled implicit solvers and segregated fluid isothermal and coupled energy. The wall treatment (All-y$^+$) and turbulence model (Realizable $k-\epsilon$) were chosen according to the mesh dependence study conducted by Van der Merwe (2014), due to the reduction in computational resources required in comparison to Large Eddy Simulations.

3.2.5 Solvers and stopping criteria

The default settings for the segregated and coupled flow models as well as the segregated fluid isothermal and coupled energy models were used for all the simulations. Segregated flow and segregated fluid isothermal energy were used for the first 500 iterations, which ensured that all residuals were under 10^{-3}; after which the coupled implicit flow and coupled energy models were used for an additional 1000 iterations.

This change in flow solvers was chosen because it was found that the segregated solver could lower the residuals below 10^{-3} after about 200 iterations for most Reynolds numbers. The coupled solver took much longer to produce converged results under 10^{-3}, but the coupled solver produced pressure drops which were closer to values predicted by correlations. Therefore, the simulations were initialised with the segregated flow solver, after which it was switched to the coupled flow solver.

3.2.6 Mesh dependence study - Wentz and Thodos (1963) experiments

The goal of the mesh dependence study was to find an appropriate base size of the volume mesh to determine the pressure drop through a body-centred cubic packed pebble bed of porosity $\epsilon = 0.383$. To this end, the physics continua settings were kept the same for all simulations, with only the base size being varied. Various Reynolds numbers at the inlet were tested, with the velocity profile for a certain Reynolds number kept constant between the various base size meshes. The methodology of the mesh independence study will be discussed in this subsection.

3.2.6.1 Mesh generation

The mesh over the domain was found to have a significant effect on the pressure drop obtained over a packed pebble bed. The fineness of the mesh was adapted by changing the base size.

During the CFD simulations, it was found that the residuals were too high (above 1) if the surface size of the mesh was kept constant over the entire control volume. Upon further research, it was determined that by choosing a smaller surface mesh size over the packed region, the simulation would be more stable, and convergence of the simulation could be achieved at a faster rate (Van der Merwe, 2014). Therefore, the surface mesh size was chosen as $0.1B$.

The base sizes (in millimetre) that were chosen to conduct the mesh dependence study are given in Table 3.2-3:

Table 3.2-3: Base sizes used for the Wentz and Thodos (1963) mesh dependence study and the resultant number of cells

Base size (mm)	Surface mesh size over packed bed (mm)	Number of cells
7.5	0.75	14207581
10	1	4515590
15	1.5	4418213
20	2	3967797
30	3	3198587
40	4	3074967
50	5	3003719

An example of a generated volume mesh (base size of 50 mm) for the Wentz and Thodos (1963) mesh dependence study is shown in Figure 3.2-2:

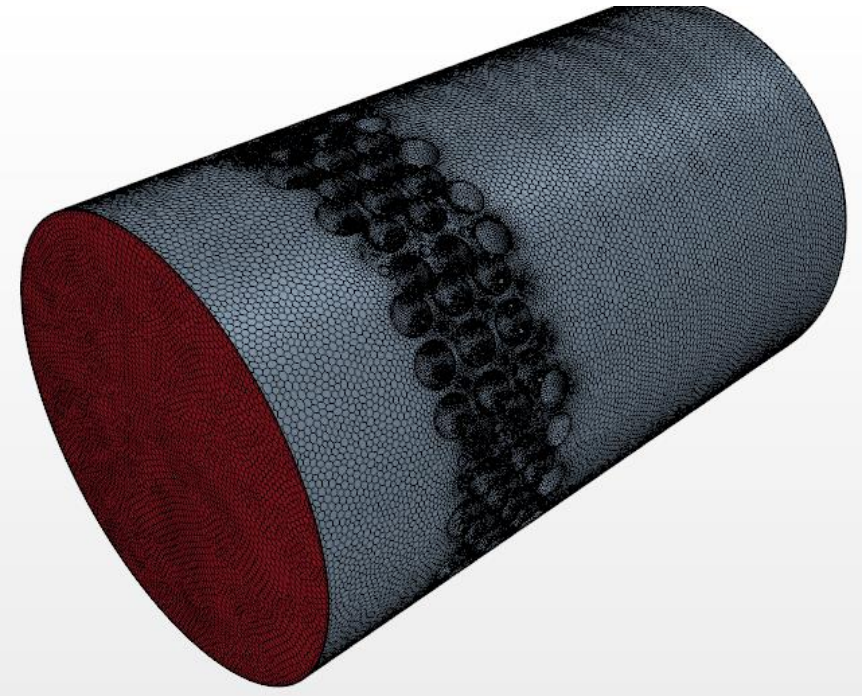

Figure 3.2-2: Volume mesh generated for a base size of 50 mm

3.2.6.2 Physics continua

The physics continua were set according to Section 3.2.4. The goal of the mesh dependence study was to determine the influence of the mesh fineness on the pressure drop of a fluid flowing through the packed bed; therefore, the physics continua were kept constant for all simulations.

During testing of the higher Reynolds numbers ($Re_p \geq 4000$), it was found that the solver was unstable, and convergence could not be achieved, if the simulations were initialized with coupled flow. Therefore, the simulations were initialized with the segregated flow and segregated isothermal energy models and ran for 500 iterations before the coupled flow and energy flow models were selected, after which the simulations were run for another 1000 iterations.

3.2.6.3 Reynolds numbers of the fluid flowing through the Wentz and Thodos (1963) simulated structured packed beds

As stated previously, the simulations were tested for several Reynolds numbers. This was done to compare the results with the pressure drop and friction factor correlations proposed by Wentz and Thodos (1963), as well as the corresponding correlations proposed by the KTA (1981). The Reynolds numbers used in the mesh dependence study are given in Table 3.2-4:

Table 3.2-4: Reynolds numbers used for the Wentz and Thodos (1963) mesh dependence study

Re_m	Re_p
10	6.2
20	12.3
40	24.7
162.1	100
200	123.4
400	246.8
6483.6	4000
9680.8	5972.5
32417.9	20000

3.2.6.4 Velocity profiles

Velocity profiles were specified at the inlet region in the Star-CCM+ simulations. From the literature, it was found that a radial velocity profile at the inlet was needed to have fully developed flow at the packed bed and to keep the inlet length at three particle diameters (Eppinger, et al., 2011). The velocity profiles for laminar and turbulent flows differed significantly and will be discussed below. For both the laminar and turbulent flows, an average and maximum velocity of the fluid was needed. The average velocity (V_{avg}) was solved from the equation for the particle Reynolds number:

$$Re_p = \frac{\rho V_{avg} d_p}{\mu} \tag{3.13}$$

And the modified Reynolds number:

$$Re_m = \frac{\rho V_{avg} d_p}{\mu(1-\epsilon)} \tag{3.14}$$

Dependent on which type of Reynolds number was being tested for. The Reynolds number of the pipe flow was calculated using Eq. (3.15):

$$Re = \frac{\rho V_{avg} D}{\mu} \tag{3.15}$$

Where D is the diameter of the bed.

3.2.6.4.1 Laminar flow velocity profiles

The flow in a pipe is considered laminar if the Reynolds number is below 4000 (Munson, et al., 2013). The maximum velocity was calculated using Eq. (3.16):

$$V_{max} = 2V_{avg} \tag{3.16}$$

And the laminar radial velocity was calculated using Eq. (3.17):

$$V(r) = V_{max}\left(1 - \frac{r}{R}\right) \tag{3.17}$$

With *r* the radial coordinate and *R* the radius of the pipe (Munson, et al., 2013).

3.2.6.4.2 Turbulent flow velocity profile

Since there is no general agreement on the Reynolds number for the flow regimes in a packed bed, it is assumed that no transition zone exits for the flow, and the flow in the pipe is considered turbulent if the Reynolds number is above 4000 (Munson, et al., 2013). The maximum fluid velocity was calculated using Eq. (3.18):

$$V_{max} = V_{avg}\left(\frac{(2n+1)(n+1)}{2n^2}\right) \tag{3.18}$$

The turbulent flow radial velocity profiles were calculated from Eq. (3.18):

$$V(r) = V_{max}\left(1 - \frac{r}{R}\right)^{\frac{1}{n}} \tag{3.19}$$

With *n*, the power law exponent, being calculated from the friction factor equation:

$$n = \frac{1}{\sqrt{f}} \tag{3.20}$$

Where f is calculated from the friction factor for smooth pipes (Munson, et al., 2013):

$$f = (100 \cdot Re)^{-0.25} \tag{3.20a}$$

3.2.6.5 Pressure drop measurement

The pressure drop of the fluid flowing through the packed bed was calculated from the Pressure Drop report option in Star-CCM+. This option allows the user to obtain the calculated pressure drop over the volume mesh by specifying a high- and low-pressure area. The inlet was chosen

as the high-pressure area, and the outlet was chosen as the low-pressure area. This meant that the pressure drop could be calculated for the entire system.

3.2.6.6 Friction factor calculation

As mentioned in Section 1.1, the pressure drops of the fluid flowing through the packed beds of the CFD simulations were used to calculate the friction factors according to the Blake (1922) friction factor correlation. These simulation friction factors were then compared with friction factors calculated from the correlations of Ergun (1952), Wentz and Thodos (1963), the KTA (1981) and Eisfeld and Schnitzlein (2001).

3.3 CFD Simulation Methodology - Pressure Drop Test Section (PDTS)

In this section the details of the CFD simulation setup which was used to model the Pressure Drop Test Section (PDTS) experiments are discussed. The PDTS experiments were conducted by varying the pressure at the inlet, but keeping the velocity constant, to vary the Reynolds number of the flow. Nitrogen was pumped through packed beds of body-centred cubic structure with porosities of $\epsilon = 0.36$, $\epsilon = 0.39$ and $\epsilon = 0.45$ respectively, and the pressure drop of the nitrogen was obtained by measuring difference between the inlet and outlet pressures (Du Toit & Rousseau, 2014).

The simulations were run with an implicit unsteady method. The default values for the physics and mesh continua in Star-CCM+ version 12.02.011 were used unless otherwise stated. This methodology was based on the methodology developed by Vermaak (2019), with changes made to the flow solver and mesh continua parameters. The reasoning for these changes will be discussed in the relevant subsections. Note that the focus of the study by Vermaak (2019) was to determine fluid thermal dispersion as a result of the turbulent mixing taking place. Vermaak (2019), therefore, did not pay attention to the optimization of the pressure drop over packed beds.

3.3.1 Geometry

The PDTS geometry was created in SolidWorks 2016 and was used to establish a domain over which a mesh could be created in Star-CCM+. The geometry consists of solid spheres which reflect the centroid data available for the three different porosity beds, surrounded by a solid square duct. The cross-section of the beds used in the simulations were a quarter of the size of the original bed cross-section, shown in Figure 3.3-1:

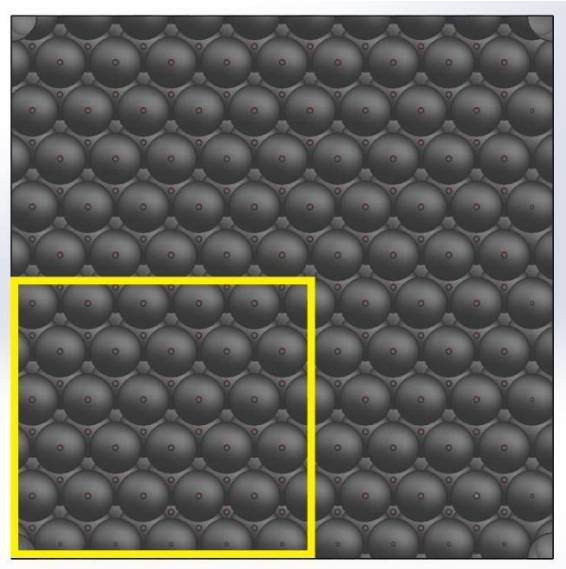

Figure 3.3-1: PDTS cross-section showing the cross-section used in Star-CCM+ in yellow.

The red outlined region in the lower left quadrant in Figure 3.3-1 shows the cross-section of the bed used in the Star-CCM+ simulations. Furthermore, the PDTS experimental beds consisted of thirty (30) axial layers of spheres, whilst the simulated beds only consisted of fifteen (15) layers, with cables being modelled between the spheres as in the actual PDTS experimental beds. Figure 3.3-2 shows the fifteen axial layers of spheres used to simulate the PDTS experiments:

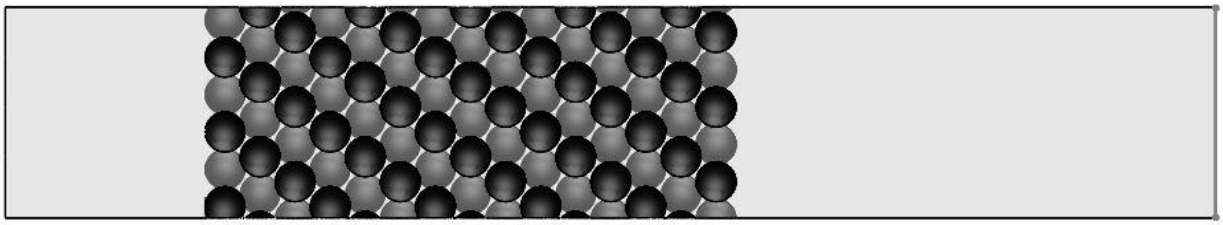

Figure 3.3-2: PDTS039 bed side view

As in Section 3.2.1, the PDTS domain was also split into regions: the inlet, packed bed, outlet, symmetry planes and walls, as shown in Figure 3.3-3 and Figure 3.3-4:

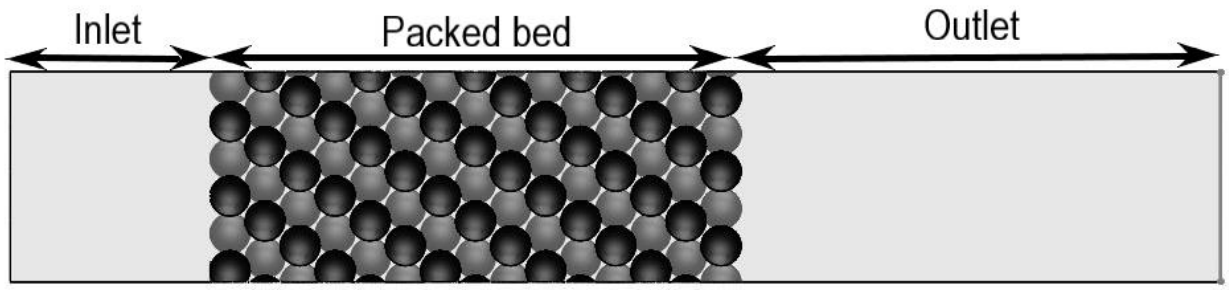

Figure 3.3-3: Geometry used in Star-CCM+ shown as the divided regions

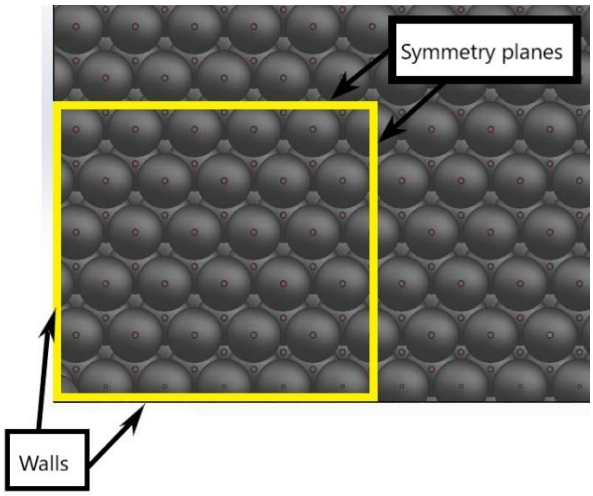

Figure 3.3-4: Cross-sectional image of the PDTS bed showing the walls and symmetry planes

The inlet extended five particle diameters upstream from the bed, and the outlet extended 12 particles downstream from the bed. The former was chosen to allow for a sufficient duct length over which the flow could develop, and the latter was chosen to eliminate the end effects of the pipe.

As mentioned earlier in this subsection, the experimental Pressure Drop Test Sections consisted of spheres in a BCC configuration with the porosity being maintained by fixing the spheres on cables. It was found that the cables influenced the pressure drop over the beds, where the geometry without cables had slightly lower pressure drops and friction factors. Du Toit and Rousseau (2014) assumed that the influence of the cables on the pressure drop of the nitrogen flowing through the bed was negligible. The difference in the friction factor (Eq. (2.7)) percentage errors between simulations modelled with and without cables between the spheres are shown in Table 3.3-1:

Table 3.3-1: Difference in the friction factors between models with and without cables for PDTS036

Model	Wall Treatment	Prism layers	Prism layer thickness (%)		Ψ % Error		
			Global	Bed	PL4	PL7	PL11
No cables	Low y^+	5	20	10	9.85	-8.4	27.8
Cables	Low y^+	5	20	10	-5.5	4.6	31.9
No cables	All y^+	3	15	5	-20.11	-8.5	22.85
Cables	All y^+	3	15	5	-16.76	-6.74	15.8
No cables	All y^+	2	10	2.5	42.9	35.3	16.4
Cables	All y^+	2	10	2.5	38.8	29.4	10.9

As can be seen in Table 3.3-1, the models including the cables generally had slightly improved friction factors when compared with the experimental results. Therefore, it was decided to use the geometry with cables when simulating the PDTS pressure drop experiments.

3.3.2 Boundaries

As mentioned in Section 3.3.1, the domains of the PDTS Star-CCM+ simulations were divided into five regions with the boundary conditions specified as in Table 3.3-2:

Table 3.3-2: Regions of the PDTS simulation domains and their respective boundary conditions

Region	Boundary conditions
Inlet	Velocity inlet
Packed bed	No-slip wall
Outlet	Pressure outlet
Walls	No-slip wall
Symmetry planes	Symmetry plane

No velocity profiles were created for the inlets: a uniform velocity and temperature was specified at the inlet, which then allowed the flow to develop over the course of the unsteady simulation. The pressure at the outlet was chosen as 0 Pa, and the outlet temperature was specified as a field function. The control volume was chosen as adiabatic, with no heat transfer modelled over the simulation boundaries. The reference pressure varied according to the pressure level being simulated.

3.3.3 Mesh continua

The mesh continua were based on those suggested by Vermaak (2019), and the following meshing models were used:

- Surface remesher
- Polyhedral volume mesher
- Prism layer mesher

All volume meshes were meshed with a fine tessellation density. Table 3.3-3 displays some of the parameters that were used to generate the mesh for the PDTS simulations:

Table 3.3-3: PDTS simulation mesh parameters

Parameter	Value
Base size, B	4 mm
Minimum surface size (global)	$0.25B$
Target surface size (global)	$1.00B$
Minimum surface size (bed)	$0.2B$
Target surface size (bed)	$0.25B$
Surface growth rate	1.3
Surface curvature	72 points per circle
Number of prism layers	Varies
Prism layer thickness	Varies
Tet/poly density	1.2
Tet/poly growth rate	0.85

The mesh continua parameters shown in Table 3.3-3 were found by Vermaak (2019) to generate high-quality meshes, therefore it was decided to use the same parameters for this section of the study. The number of prism layers were varied for the different pressure levels, due to a larger number of prism layers resulting in an over-prediction of the pressure drop through the bed. The prism layer thickness over the packed bed was usually thinner than that used globally, unless otherwise stated.

3.3.4 Physics continua

For the PDTS validation simulations, the physics continua were kept constant when modelling the various pressure levels. The following physics continua were as follows:

- Implicit unsteady.
- Three dimensional.
- Ideal gas: Nitrogen (N_2).
- Segregated flow solver.
- Segregated fluid temperature.
- All-y^+ wall treatment.
- Turbulent.
- Large Eddy Simulation.
    - WALE subgrid scale.

Large Eddy Simulation was chosen as the turbulence model because it was found that Reynolds-Averaged Navier-Stokes turbulence models did not converge at the higher Reynolds numbers. The pressure of the specific pressure level at which the flow was being modelled was specified as the reference pressure in the physics continua. The reference pressures for the pressure levels that were modelled for each porosity are shown in Table 3.3-4:

Table 3.3-4: Reference pressure used for the PDTS simulations

Model	Reference Pressure (Pa)		
	Pressure level 4	**Pressure level 7**	**Pressure level 11**
PDTS036	399637.873	698109.763	1997603.733
PDTS039	400386.571	700169.53	2000363.167
PDTS045	399202.083	700465.438	1998260.133

The high pressure of the nitrogen used in the PDTS experiments caused the density of the nitrogen to be very high, as shown in Table 3.3-5:

Table 3.3-5: PDTS experimental densities

Model	Density ($\frac{kg}{m^3}$)		
	Pressure level 4	**Pressure level 7**	**Pressure level 11**
PDTS036	4.664	8.155	23.407
PDTS039	4.589	8.03	22.986
PDTS045	4.541	8.062	23.045

3.3.5 Inlet temperature and velocity specifications

As mentioned in Section 3.3.2, the inlet was specified as a Velocity Inlet region. The temperature and velocity of the fluid flowing over the bed was specified at this region. The inlet velocities and temperatures of the fluid used for the PDTS simulations were chosen according to the PDTS experimental data, as shown in Table 3.3-6 and 3.3-7, respectively:

Table 3.3-6: Inlet velocities at each pressure level for the PDTS simulations

Model	Inlet velocity (m/s)		
	Pressure Level 4	Pressure Level 7	Pressure Level 11
PDTS036	0.521	0.524	0.531
PDTS039	0.539	0.541	0.546
PDTS045	0.548	0.537	0.544

Table 3.3-7: Inlet temperature at each pressure level for the PDTS simulations

Model	Inlet temperature (˚C)		
	Pressure Level 4	Pressure Level 7	Pressure Level 11
PDTS036	15.832	15.821	15.739
PDTS039	21.062	21.065	21.152
PDTS045	23.283	20.047	20.136

3.3.6 Solvers and stopping criteria

Because the flow for these simulations was simulated for a transient (unsteady) state, the flow field first had to develop. This was done by simulating the flow with a relatively large time-step of one second for the first thousand iterations. One time-step was equivalent to twenty-five iterations. After the first thousand iterations, the time-steps were reduced to smaller increments, up to time-step reductions on the order of milliseconds. The last time-step increment size corresponded to the Courant-Friedrichs-Lewy (CFL) flow stability condition, which is defined as:

$$C = \frac{u\Delta t}{\Delta x} \leq 1 \tag{3.20}$$

Where C is the dimensionless convective Courant number, u is the velocity in meter per second, Δt is the time-step in seconds, and Δx is the cell size in meter. The velocity and cell size are kept constant, which means that the condition of $C \leq 1$ can only be satisfied by changing the time-step. A Courant number close or equal to 1 means that the flow moved from one cell centroid to the next in time step – this results in increased simulation stability. The time-step reduction

process is shown in Table 3.3-8. The CFL satisfying time-step shown below was not constant for all Reynolds numbers: for the lowest Reynolds numbers ($Re_p = 1000$), the CFL satisfying time-step was typically achieved at $\Delta t = 0.1\ s$, whilst at high Reynolds numbers ($Re_p = 50000$) the CFL satisfying time-step usually achieved at $\Delta t = 0.004\ s$.

Table 3.3-8: Time-step reduction overview for the PDTS simulations

Iteration		Time-step (s)
Initial	**Final**	
0	1000	1
1000	1100	0.5
1100	1200	0.1
1200	1300	0.07
1300	1400	0.04
1400	1500	0.01
1500	1600	0.008
1600	1700	0.006
1700	1800	0.004
1800	1900	0.002
1900	2000	0.001
2000	5000	CFL time-step

3.4 PDTS Mesh Refinement

As stated in Section 1.4, the objectives of this section of the study was to determine whether it is possible to use CFD simulations to accurately model the pressure drop experiments of the Pressure Drop Test Sections. The geometries used for these pressure drop simulations were similar to those used by Vermaak (2019). Furthermore, Vermaak (2019) completed a mesh dependence study for the geometry used for the PDTS simulations, therefore the mesh continua were based on his findings and recommendations. The original goal was to find a mesh which could be universally applied to give accurate results at three pressure levels for all three porosities, namely pressure levels 4, 7 and 11.

However, during initial testing, it was found that the mesh continua settings given by Vermaak (2019), particularly the number of prism layers and the prism layer thickness, were unsuited to provide accurate results for all three pressure levels. This is shown in Table 3.4-1, where two meshes with differing number of prism layers and prism layer thickness were used to calculate the friction factor for PDTS036:

Table 3.4-1: Friction factor percentage errors for different prism layer values for the PDTS036 simulation

Prism Layers	Prism layer thickness (%)		Ψ Percentage Error (%)		
	Global	Bed	Pressure level 4	Pressure level 7	Pressure level 11
2	10	5	38.4	29.4	10.9
5	20	10	-5.19	4.6	32.3

As can be seen in Table 3.4-1, pressure levels 4 and 7 could be modelled more accurately using a mesh with more prism layers with a larger thickness, whilst pressure level 11 was modelled more accurately using fewer prism layers with a much lower thickness. It was postulated that this was due to the boundary layer over the spheres being thicker at lower Reynolds numbers, such as at pressure levels 4 and 7 (which had particle Reynolds numbers of $Re_p = 4000$ and $Re_p = 7000$, respectively), which would be better resolved with thicker and more prism layers. On the contrary, the boundary layer would become thinner at higher Reynolds numbers, such as at pressure level 11 (which had a particle Reynolds number of $Re_p = 20000$), which would result in the prism layer reaching into the free-flow area between the spheres, consequently over-predicting the pressure drop. Therefore, it became apparent that each pressure level had to have its specific own mesh generated.

Furthermore, it was also initially thought that the mesh continua parameters (specifically the prism layer settings) which generated accurate results for each pressure level for PDTS036 would also give accurate results when used at the same pressure level for the other two Pressure Drop Test Sections – PDTS039 and PDTS045. In other words, the mesh continua parameters which generated accurate results at pressure level 11 for PDTS036 would also give accurate results at Pressure Level 11 for both PDTS039 and PDTS045. This was found not to be true, as can be seen in Table 3.4-2:

Table 3.4-2: Friction factors for the various Pressure Drop Test Sections at PL11 with identical mesh continua

Porosity	Prism Layers	Prism layer thickness (%)		Ψ Percentage Error (%) at PL11
		Global	Bed	
PDTS036	3	12.5	3.75	0.5
PDTS039				-11.3
PDTS045				-21.6

This increased deviation in the percentage error could be caused by the higher porosities having a wider lateral distance between spheres, resulting in an increased channelling effect. This

increased channelling effect could result in thicker boundary layers, which thin prism layers cannot resolve as accurately as thicker prism layers. It was then apparent that each Pressure Level which needed to be simulated for the specific Pressure Drop Test Section had to have its own individual mesh generated.

The unique mesh settings for each specific pressure level were determined by varying the prism layer thickness and number of prism layers globally as well as in the bed; by simulating the flow conditions at each pressure level using the mesh and physics continua established in Sections 3.3.3 and 3.3.4, respectively.

3.5 Summary

In this chapter, the methodologies used during the two separate studies of the analysis of the pressure drop over a structured packed bed was discussed. The analysis was conducted using the numerical CFD simulation program Star-CCM+ to model the flow explicitly through structured packed beds.

The methodology used to simulate the flow through packed beds similar to those used by Wentz and Thodos (1963) was an evolution of the methodology established by Van der Merwe (2014), whilst the original methodology used to analyse the pressure drop over the PDTS beds was established by Vermaak (2019). The geometry used for these studies and how they were meshed and divided into regions were described. The physics and mesh continua of the simulations for both sets of simulations and the reasoning behind the particular choices were described. The results obtained from the methodologies used in these simulations will be given in the next chapter.

CHAPTER 4: RESULTS

This chapter will show and discuss the results obtained from both the Wentz and Thodos (1963) as well as the PDTS simulations of the flow through the respective CAD generated packed beds. The Wentz and Thodos (1963) and the PDTS simulations were executed according to the methodologies developed in Sections 3.2 and 3.3, respectively. The results obtained from the simulations show the effect that the mesh and flow parameters, such as the Reynolds number, have on the pressure drop of the flow through a packed bed.

4.1 Wentz and Thodos (1963) Mesh Independence study

The base sizes of the volume mesh specified in Section 3.2.6.1 were each simulated for all eight Reynolds numbers in the bed specified in Section 3.2.6.3. The results of these simulations will be discussed in this section. Each table will show the Reynolds number being simulated, the resultant pressure drop of the specific simulation, and the friction factor as calculated using Eq. (2.7) as given in Section 2.3.

4.1.1 Star-CCM+ validation of the results obtained by Van der Merwe (2014)

As stated in Section 1.4, the first objective of this study was to determine whether the results generated for the Wentz and Thodos (1963) simulations by Van der Merwe (2014) in Star-CCM+ version 7 could be generated with a reasonable degree of accuracy using Star-CCM+ version 12.

Van der Merwe (2014) simulated the flow through the geometry for several particle Reynolds numbers. The mesh used by Van der Merwe had a base size of 36 mm, a refined mesh base size over the pebbles of 3.6 mm, with 2 prism layers over all regions defined as non-slip walls. Van der Merwe (2014) meshed and simulated the flow over the bed in Star-CCM+ version 7.

The CFD program used in this study was Star-CCM+ version 12, which is a much more recent version. This raised the question whether the meshes generated in this version, as well as the simulations, may differ significantly from the older version. Therefore, it was decided to generate the mesh in Star-CCM+ version 12 according to the same mesh continua parameters specified by Van der Merwe (2014). The meshed geometry would then be simulated under the same flow conditions as the simulation performed by Van der Merwe (2014) to compare the results that were generated by Star-CCM+ version 7 and 12.

The simulation that was chosen for comparison was for a particle Reynolds number of 4800. The superficial velocity at the inlet 2.426 m/s, and the fluid used was air at standard temperature and pressure. The pressure drops for the two simulations are shown in Table 4.1-1:

Table 4.1-1: Comparison in pressure drop between Star-CCM+ version 7 and 12

Pressure drop (Pa)		Percentage difference (%)
Star-CCM+ version 7 (Van der Merwe, 2014)	***Star-CCM+ version 12***	
339.99	341.28	0.38

In Table 4.1-1, it is shown that the pressure drops predicted by Star-CCM+ version 7 and Star-CCM+ version 12 compare very closely, differing by only 0.38%. This indicates that Star-CCM+ version 12 can be used for further simulations.

4.1.1.1 Re_m = 10

These simulations were executed with an intended modified Reynolds number of 10, with an inlet Reynolds number of 70.22. The flow in the bed was laminar, therefore the average velocity, maximum velocity and radial velocity were calculated by using equations (3.14), (3.16) and (3.17), respectively. The average velocity was calculated as $V_{avg} = 3.117 \times 10^{-3} \frac{m}{s}$, and the maximum velocity as $V_{max} = 6.234 \times 10^{-3} \frac{m}{s}$. The pressure drops and friction factors for $Re_m = 10$ as a function of the base size are shown in Table 4.1-2:

Table 4.1-2: Pressure drop for the various base sizes for Re_m=10

Base size (mm)	Pressure drop (Pa)	Ψ_{Blake}
7.5	0.01556	64.05
10.0	0.01564	64.37
15.0	0.01565	64.41
20.0	0.01559	64.13
30.0	0.01559	64.13
40.0	0.01600	65.84
50.0	0.01610	66.25

From Table 4.1-2, it is apparent that the pressure drops for each base size lies close to one another. The pressure drop predicted by the simulations with base mesh sizes of 40 and 50 millimetres, respectively, gave slightly higher pressure drops than the other base sizes. The mean pressure drop for $Re_m = 10$ was 0.0157325 Pa, with a standard deviation of 0.2212×10^{-3} Pa,

whilst the average friction factor of the flow was 64.74, with a standard deviation of 0.91. This means that the standard deviation of both the pressure drop and friction factor is only 1.4% from the mean. Only the base sizes of 40 and 50 mm fell outside one standard deviation from the mean.

4.1.1.2 Re_m = 20

These simulations were performed with an intended modified Reynolds number of 20, with an inlet Reynolds number of 140.44. Since the flow in the bed was laminar, the average velocity, maximum velocity and radial velocity were calculated using Eqs. (3.14), (3.16) and (3.17), respectively. The average velocity was calculated as $V_{avg} = 6.234 \times 10^{-3} \frac{m}{s}$, and the maximum velocity as $V_{max} = 12.468 \times 10^{-3} \frac{m}{s}$. The pressure drops and frictions factors as functions of base sizes are shown in Table 4.1-3:

Table 4.1-3: Pressure drop for the various base sizes for Re_m=20

Base size (mm)	Pressure drop (Pa)	Ψ_{Blake}
7.5	0.02532	26.05
10.0	0.02358	24.26
15.0	0.02331	23.98
20.0	0.02365	24.33
30.0	0.02409	24.79
40.0	0.02360	24.28
50.0	0.02349	24.17

Table 4.1-3 shows the pressure drops predicted by the simulations with the meshes generated for the various base sizes for a modified Reynolds number of $Re_m = 20$, and most of the pressure drops lie close to each other. The exception is the base size of 7.5 mmm, which predicted a pressure drop higher than the rest. The mean pressure drop for $Re_m = 20$ was 0.023864 Pa, with a standard deviation of 0.684×10^{-3} Pa. The mean friction factor at this flow was 24.55, with a standard deviation of 0.7. Both the pressure drop and friction factor standard deviations are 2.86% from the mean. All the pressure drops for the base sizes fell within one standard deviation from the mean, except for the base size of 7.5 mm. It should also be noticed that as the base size increases from 7.5 mm, the pressure drop drops slightly, before rising, and then drops again after a base size of 30 mm.

4.1.1.3 Re_m = 40

These simulations were executed with an intended modified Reynolds number of 40, and an overall Reynolds number of 280.88. The flow in both the cylinder and bed were laminar, the average velocity, maximum velocity and radial velocity were calculated using equations (3.14), (3.16) and (3.17). The average velocity was calculated as $V_{avg} = 12.468 \times 10^{-3} \frac{m}{s}$, and the maximum velocity as $V_{max} = 24.936 \times 10^{-3} \frac{m}{s}$. The pressure drops and friction factors obtained from the simulations are shown in Table 4.1-4 as a function of the base size:

Table 4.1-4: Pressure drop for the various base sizes for Re_m=40

Base size (mm)	Pressure drop (Pa)	Ψ_{Blake}
7.5	0.0625	16.07
10.0	0.0625	16.08
15.0	0.0547	14.09
20.0	0.0544	13.99
30.0	0.0512	13.17
40.0	0.0469	12.05
50.0	0.0450	11.57

Table 4.1-4 shows the pressure drops and friction factors obtained for the base sizes for a modified Reynolds number of $Re_m = 40$. One again, the base size of 7.5 mm predicted a pressure drop higher than the rest, but equal to the pressure drop predicted for a base size of 10 mm, after which the pressure drop consistently decreased as the base size increased. The mean pressure drop was 0.05389 Pa, and the standard deviation for the pressure drops was 6.8975×10^{-3} Pa, which is 12% from the mean. The mean friction factor for the simulations was 13.86, with a standard deviation of 1.77; which, like the standard deviation of the pressure drop, falls within 12% from the mean. The pressure drops predicted by the base sizes of 7.5, 10 and 50 mm fall outside one standard deviation from the mean.

4.1.1.4 Re_m = 162

These simulations were executed with an intended modified Reynolds number of 162, and an inlet Reynolds number of 1138. Since the flow in the bed was laminar, the average velocity, maximum velocity and radial velocity were calculated using equations (3.13), (3.16) and (3.17). The average velocity was calculated as $V_{avg} = 0.051 \frac{m}{s}$, and the maximum velocity as $V_{max} = 0.101 \frac{m}{s}$. The pressure drops and friction factors as a function of the base size for a flow at $Re_m = 162$ are shown in Table 4.1-5:

Table 4.1-5: Pressure drop for the various base sizes for Re_m=162

Base size (mm)	Pressure drop (Pa)	Ψ_{Blake}
7.5	0.391	6.12
10.0	0.390	6.11
15.0	0.382	5.99
20.0	0.374	5.85
30.0	0.357	5.59
40.0	0.320	5.01
50.0	0.360	5.63

Table 4.1-5 shows the pressure drops predicted by the simulations for the meshes of the various base sizes for a modified Reynolds number of $Re_m = 162$. The pressure drops lie close to one another, except for the pressure drop predicted for the base size of 40 mm. The mean pressure drop was 0.36773 Pa, and the standard deviation was 0.024956 Pa. The mean friction factor calculated for the simulations was 5.76, with a standard deviation of 0.39. Both the friction factor and pressure drop standard deviations fell within 6.79% of the mean. Only the pressure drop predicted by the base size of 40 mm falls outside of one standard deviation from the mean. The predicted pressure drops decrease as the base size increases from 7.5 mm.

4.1.1.5 Re_m = 200

These simulations were run with an intended modified Reynolds number of 200 and an inlet Reynolds number of 1404.4. This modified Reynolds number indicates laminar flow; therefore, the average velocity, maximum velocity and radial velocity was calculated using equations (3.14), (3.16) and (3.17), respectively. The average velocity was calculated as $V_{avg} = 0.062\frac{m}{s}$, and the maximum velocity as $V_{max} = 0.125\frac{m}{s}$. The pressure drops as a function of the base size is shown in Table 4.1-6:

Table 4.1-6: Pressure drop for the various base sizes for Re_m=200

Base size (mm)	Pressure drop (Pa)	Ψ_{Blake}
7.5	0.541	5.57
10.0	0.531	5.46
15.0	0.531	5.46
20.0	0.510	5.24
30.0	0.487	5.01
40.0	0.492	5.06
50.0	0.492	5.06

Table 4.1-6 shows the pressure drops predicted by the simulations for the meshes of the various base sizes for a particle Reynolds number of $Re_m = 200$. As with $Re_p = 100$, the pressure drop predicted by the base size of 7.5 mm was the highest. The mean pressure drop was 0.512 Pa, with a standard deviation of 0.022 Pa, and the mean friction factor was 5.27, with a standard deviation of 0.24. Both the pressure drop and friction factor standard deviations were 4.38% from the mean. The pressure drop predicted for the base sizes of 7.5 and 30 mm fell outside one standard deviation of the mean. From Table 4.1-6, it can be seen that the predicted pressure drops decrease slightly from the maximum predicted by the 7.5 mm base size.

4.1.1.6 Re_m = 400

These simulations were run with an intended modified Reynolds number of 400, with an inlet Reynolds number of 2808.84. The flow in the bed had begun to transition from laminar to turbulent but was still considered to be close to the laminar flow upper limit. Therefore, the average velocity, maximum velocity and radial velocity were calculated using Eqs. (3.14), (3.16) and (3.17), which were the laminar velocity equations. The average velocity was calculated as $V_{avg} = 0.127\frac{m}{s}$, and the maximum velocity as $V_{max} = 0.249\frac{m}{s}$. The predicted pressure drops and friction factors for the base sizes are shown in Table 4.1-7:

Table 4.1-7: Pressure drop for the various base sizes for Re_m=400

Base size (mm)	Pressure drop (Pa)	Ψ_{Blake}
7.5	1.677	4.31
10.0	1.665	4.28
15.0	1.576	4.05
20.0	1.481	3.81
30.0	1.437	3.70
40.0	1.465	3.77
50.0	1.467	3.77

Table 4.1-7 gives the pressure drops predicted by the simulations for the meshes of the various base sizes for a particle Reynolds number of $Re_m = 400$. As with $Re_m = 200$, the maximum pressure drop was generated for a mesh with a base of 7.5 mm, and the predicted pressure drop decreased as the base size increased. The mean pressure drop for $Re_m = 400$ is 1.5382 Pa, and the standard deviation is 0.1007 Pa, and the mean friction factor was 3.96, with a standard deviation of 0.26. Both the standard deviations of the friction factor and pressure drop were 6.55% from the mean. As with $Re_m = 200$, the base sizes of 7.5 and 30 mm predicted pressure drop one standard deviation from the mean, along with a base size of 10 mm.

4.1.1.7 Re_m = 6484

These simulations were performed with an intended modified Reynolds number of 6484, with an inlet Reynolds number of 45528.5. The flow in both the cylinder and bed were turbulent, the average velocity, maximum velocity and radial velocity were calculated using Eqs. (3.13), (3.18) and (3.19), respectively. The average velocity was calculated as $V_{avg} = 2.021\frac{m}{s}$, and the maximum velocity as $V_{max} = 2.489\frac{m}{s}$. The predicted pressure drops as a function of the base sizes are shown in Table 4.1-8:

Table 4.1-8: Pressure drop for the various base sizes for Re_m=6484

Base size (mm)	Pressure drop (Pa)	Ψ_{Blake}
7.5	219.410	2.15
10.0	213.704	2.09
15.0	215.563	2.11
20.0	217.735	2.13
30.0	222.458	2.18
40.0	224.588	2.20
50.0	226.087	2.21

Table 4.1-8 shows the pressure drops predicted by the simulations for the meshes of the various base sizes for a modified Reynolds number of $Re_m = 6484$. The pressure drop predicted for a mesh with a base size of 50 mm was the highest. The pressure drop decreases as the base size decreases from 7.5 mm, after which it increases after a base size of 10 mm. The mean pressure drop for $Re_p = 4000$ was 219.935 Pa, with a standard deviation of 4.6355 Pa, and the mean friction factor was 2.15, with a standard deviation of 0.05; both the pressure drop and friction factor standard deviations fell 2.11% from the mean. The base sizes of 10, 40 and 50 mm generated pressure drops one standard deviation from the mean.

4.1.1.8 Re_m = 9680

The intent of performing the simulations with this modified Reynolds number was to compare it to an experimental pressure drop obtained by Wentz and Thodos (1963) for $Re_m = 8940$. However, it was found that the average velocity recorded by Wentz and Thodos (1963) gave a modified Reynolds number of $Re_m = 9680$. It was therefore decided to use the average inlet velocity given by Wentz and Thodos (1963) as a reference value. The maximum velocity and radial velocity profile were calculated from equations (3.18) and (3.19), and the average velocity was specified as $V_{avg} = 3.018\frac{m}{s}$. The flow in the bed and cylinder were turbulent. The pressure drops predicted by the simulations as a function of the base size is shown in Table 4.1-9:

Table 4.1-9: Pressure drop for the various base sizes for Re_m=9680

Base size (mm)	Pressure drop (Pa)	Ψ_{Blake}
7.5	468.810	2.06
10.0	456.018	2.00
15.0	467.731	2.05
20.0	475.739	2.09
30.0	479.984	2.11
40.0	484.424	2.13
50.0	488.823	2.15

Table 4.1-9 shows the pressure drops predicted by the simulations for the meshes of the various base sizes for a modified Reynolds number of $Re_m = 9680$. The pressure drop predicted for a mesh with a base size of 50 mm was the highest. The pressure drop decreases as the base size decreases from 7.5 mm, after which it increases after a base size of 10 mm. The mean pressure drop for $Re_m = 9680$ was 474.5 Pa, with a standard deviation of 11.2175 Pa. The mean friction factor was 2.08, with a standard deviation of 0.05. The standard deviations of the pressure drops and friction factors fell 2.36% from the mean. The base sizes of 10 and 50 mm generated pressure drops one standard deviation from the mean. It should be noted that the pattern of the pressure drop for the base sizes in Table 4.1-9 (for $Re_m = 9680$) is identical to the pattern generated in Table 4.1-8 (for $Re_p = 4000$).

4.1.1.9 Re_m = 32418

These simulations were performed for an intended modified Reynolds number of 32418, and an inlet Reynolds number of 227642. The flow in the cylinder as well as the bed were turbulent. Therefore, the average velocity, maximum velocity and radial velocity were calculated using equations (3.13), (3.18) and (3.19). The average velocity was calculated as $V_{avg} = 10.105\frac{m}{s}$, and the maximum velocity as $V_{max} = 12.001\frac{m}{s}$. The pressure drops for the base sizes are shown in Table 4.1-10:

Table 4.1-10: Pressure drop for the various base sizes for Re_m=32417

Base size (mm)	Pressure drop (Pa)	Ψ_{Blake}
7.5	5219.177	2.04
10.0	5076.322	1.99
15.0	5143.662	2.01
20.0	5195.675	2.03
30.0	5229.616	2.05
40.0	5303.115	2.08
50.0	5350.553	2.10

Table 4.1-10 shows the pressure drops predicted for the meshes of the various base sizes for a modified Reynolds number of $Re_m = 32417$. The pressure drop predicted for a mesh with a base size of 50 mm was the highest. The pressure drop decreases as the base size decreases from 7.5 mm, after which it increases after a base size of 10 mm. The mean pressure drop for this case was 5216.874 Pa, with a standard deviation of 92.231 Pa. The mean friction was 2.04, with a standard deviation of 0.04. The standard deviations of the pressure drop and friction factor fell 1.77% from the mean. As with $Re_m = 9680$, the base sizes of 10 and 50 mm generated pressure drops one standard deviation from the mean.

4.1.1.10 Pressure drop analysis

The goal of the mesh dependence study was to determine the influence of the mesh fineness on the pressure drop over a packed bed with a body-centred cubic structure and a porosity of $\epsilon = 0.383$. The mesh fineness was varied by changing the base size of the mesh and keeping the other mesh continua parameters constant. The meshes were used to predict the pressure drop of air over a wide range of Reynolds numbers – from viscous to highly turbulent flow.

The pressure drop as a function of the base size are shown in Figure 4.1-1:

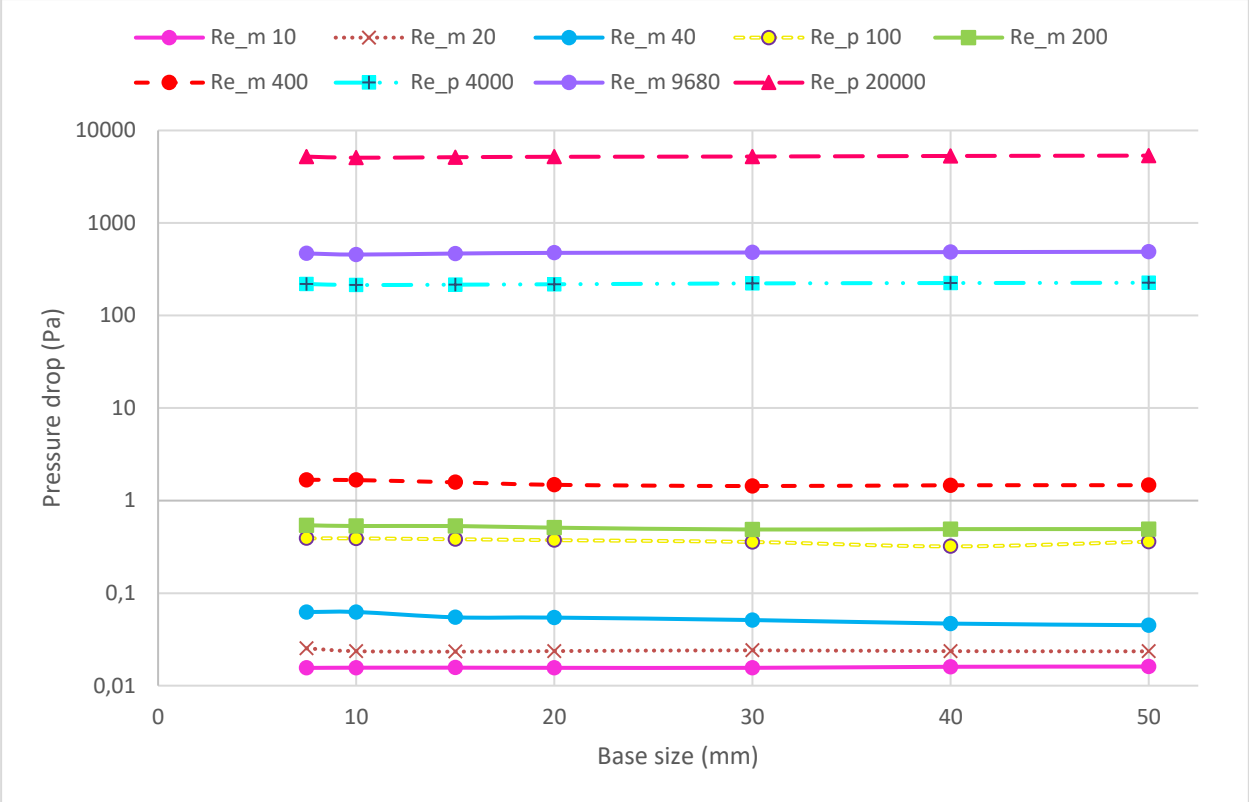

Figure 4.1-1: Pressure drop (Pa) as a function of the base size (mm) for all Reynolds numbers for the Wentz and Thodos (1963) simulations

The simulated pressure drops for all Reynolds numbers used in the simulations are shown in Figure 4.1-1, and it can be seen that the various meshes predicted pressure drops which were close to each other. In the laminar flow regime ($10 \leq Re_m \leq 400$), the highest pressure drops were predicted by the mesh with a base size of 7.5 mm, after which the predicted pressure drop decreased with an increase in the base size. Therefore, the pressure drop decreased with a decrease in the mesh fineness. In the turbulent flow regime ($6484 \leq Re_m \leq 32417$), the maximum predicted pressure drop was obtained from the mesh with a base size of 50 mm, with the pressure drop decreasing with a decrease in the base size, up to 10 mm, after which it slightly increased. Therefore, the pressure drop decreases with an increase in the mesh fineness.

The standard deviation of the pressure drops were generally less than 5% from the mean pressure drop, except for three cases: the modified Reynolds numbers of $Re_m = 40$ and $Re_m = 400$, and the particle Reynolds number of $Re_p = 100$. This means that the predicted pressure drops formed tight groups. The meshes with base sizes of 15 and 20 mm were the only meshes that predicted pressure drops within one standard deviation for all Reynolds numbers, with the rest of the meshes predicting pressure drops which fell outside one standard deviation from the mean pressure at least once.

The close spread of the predicted pressure drops and friction factors for all mesh base sizes makes it difficult to recommend a definitive base size; however, the mesh base sizes of 15 and 20 mm showed the most promise. As the mesh becomes finer, the time to find a converged solution becomes longer. Additionally, the mesh of a base size of 7.5 mm needed to be run on a much more powerful computer. This is due to the number of cells that the 7.5 mm base size mesh consists of being approximately 3 times higher on average than the other meshes. The final choice of base size will therefore be dictated by a balance between the accuracy of the solution and the available computational resources.

Additional mesh continua parameters, such as the prism layer thickness and the number of prism layers should also be investigated along with the base size. It is therefore recommended to include amongst others the effect of the prism layers on the simulated pressure drop of the fluid moving through the packed bed. Due to their statistical accuracy for all Reynolds numbers, the meshes with base sizes of 15 and 20 millimetres are the ones that show the greatest promise.

4.1.1.11 Friction factors

The validity of the results obtained with the various meshes can be better evaluated when the friction factors are compared with the friction factors of the experimental results of Wentz and Thodos (1963). This was motivated, amongst others, by the concern that the geometrical and structural properties of the simulated beds, for example the bed length, exact placing of the spheres and porosity, could not be accurately determined from the information provided by Wentz and Thodos (1963). This also gives the opportunity to compare the simulation results with friction factors predicted by the correlations proposed by Wentz and Thodos (1963), the KTA (1981), Ergun (1952) and Eisfeld and Schnitzlein (2001).

Wentz and Thodos (1963) measured pressure drops over packed beds with porosities that varied from 0.354 to 0.882, which has close packed simple cubic (SC) and body-centred cubic (BCC) packings, as well as distended beds with SC, BCC and Face-Centred Cubic (FCC) packings. The friction factors for the close packed BCC bed with a porosity of 0.354 is given in Table 4.1-11:

Table 4.1-11: Wentz and Thodos (1963) experimental friction factors for ε=0.354

Re_m	$\Psi_{W\&T\ Exp}$
2550	2.812
3140	2.792
3640	2.626
4900	2.488
6310	2.292
7150	2.252
8220	2.198
9840	2.154

The friction factors calculated using the Ergun (1952) (Eq. (2.9)), Wentz and Thodos (1963) (Eq. (2.15)), KTA (1981) (Eq. (2.17), and Eisfeld and Schnitzlein (2001) (Eq. (2.13)) correlations as functions of the modified Reynolds numbers are shown in Table 4.1-12. The range of modified Reynolds used in these calculations are based on the experimental modified Reynolds numbers used by Wentz and Thodos (1963):

Table 4.1-12: Friction factors calculated with various correlations as a function of the modified Reynolds number

Re_m	Ψ_{Ergun}	$\Psi_{W\&T}$	Ψ_{KTA}	$\Psi_{E\&S}$
2550	3.618	2.826	2.864	2.980
3140	3.596	2.678	2.784	2.953
3640	3.582	2.582	2.731	2.937
4900	3.561	2.405	2.631	2.910
6310	3.548	2.270	2.552	2.894
7150	3.542	2.209	2.515	2.887
8220	3.536	2.144	2.475	2.880
9680	3.531	2.072	2.429	2.873

In Table 4.1-12, the values of the porosity and aspect ratio used in the calculations were based on the simulation geometry values of 0.383 and 11.382, respectively.

The friction factors as a function of the modified Reynolds number from the Wentz and Thodos (1963) experiments (Exp) are shown in Figure 4.1-2. Also shown in Figure 4.1-2 are friction factors for $2550 \leq Re_m \leq 9680$ predicted by the Ergun (1952), Wentz and Thodos (1963) (W+T), KTA (1981) (KTA) and Eisfeld and Schnitzlein (2001) (E+S) correlations:

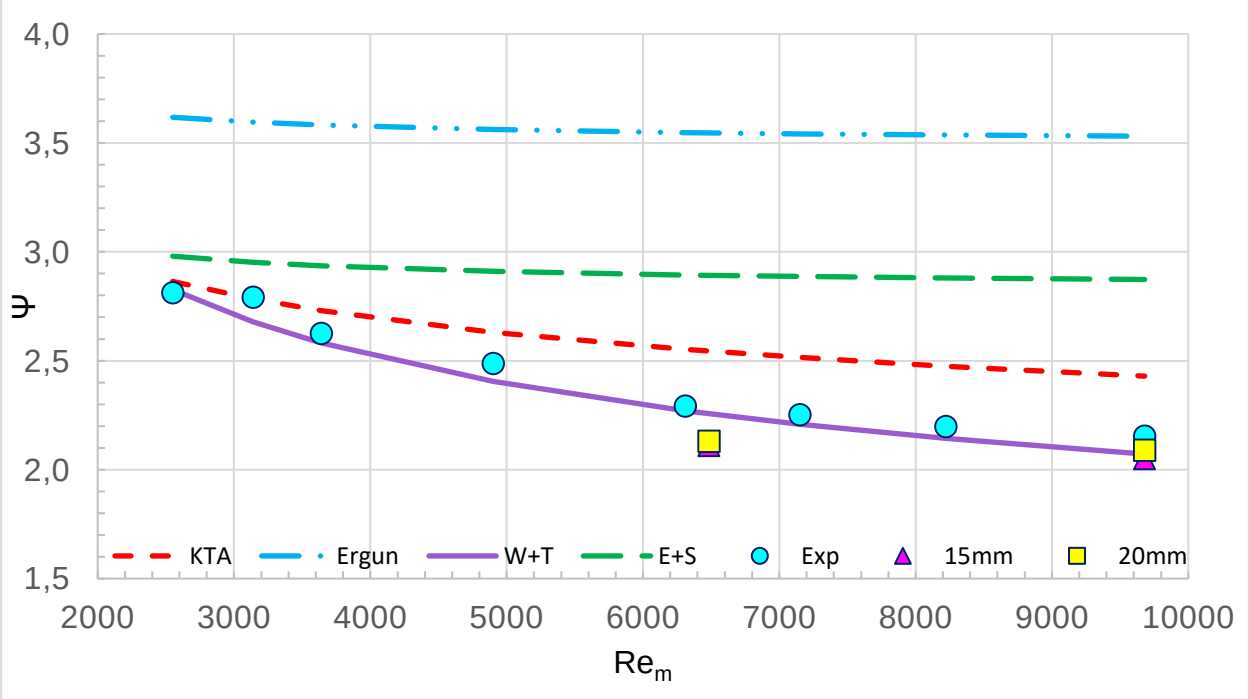

Figure 4.1-2: Wentz and Thodos (1963) experimental and correlation friction factors, as well as the friction factors calculated using the Ergun (1952), KTA (1981) and Eisfeld and Schnitzlein (2001) correlations

The discrepancy between the friction factors predicted by the Ergun (1952) correlation and Wentz and Thodos (1963) experimental values was attributed to the fact that the experimental spheres were smooth, whereas in the Ergun (1952) study the randomly packed spheres had varying degrees of rough surfaces. The KTA (1981) correlation was derived from random packed beds of spheres having a uniform size. Although the Eisfeld and Schnitzlein (2001) correlation was derived for randomly packed spheres, it is still based on the Ergun (1952) correlation. Du Toit and Rousseau (2014) concluded that for $Re_m > 300$ packing structure along with the overall porosity play an important role to determine the friction factor. From Figure 4.1-2 it can be seen that the values for the friction factors predicted by the KTA (1981) and Wentz and Thodos (1963) correlations, as well as the Wentz and Thodos (1963) experimental values begin to converge as Re_m decreases towards $Re_m = 2550$. Figure 4.1-3 also shows that the friction factors from the simulations for base sizes of 15 and 20 mm differ by 5.6% and 0.9% from the values predicted by the Wentz and Thodos (1963) correlation for $Re_m = 6482$ and $Re_m = 9680$ respectively.

Based on the conclusion that the simulation packed beds for base sizes of 15 and 20 mm are the most promising ones, as well as the conclusion that the values predicted by the KTA (1981) correlation moves closer to the Wentz and Thodos (1963) experimental values at lower modified Reynolds numbers; the simulation friction factors for 15 mm and 20 mm are compared with the values predicted by the KTA (1981) and Wentz and Thodos (1963) experimental values in Figure 4.1-3:

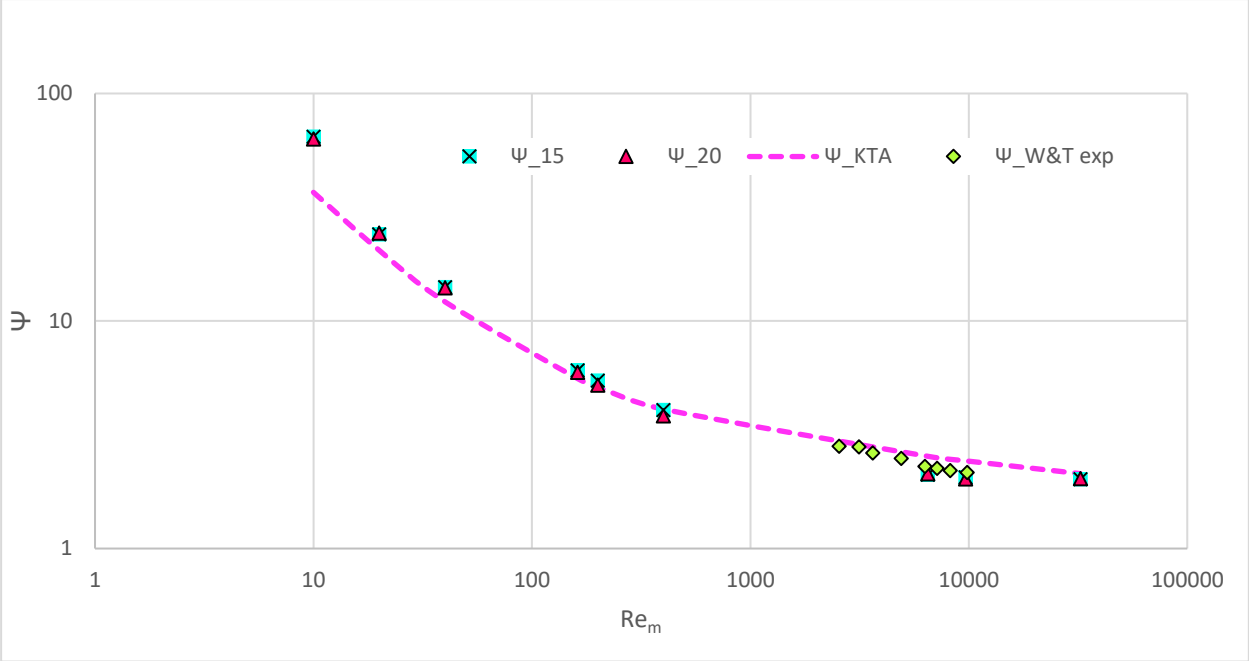

Figure 4.1-3: Friction factors for base sizes of 15 and 20 mm compared to the KTA (1981) correlation and Wentz and Thodos (1963) experimental values

It can be seen in Figure 4.1-3 that for $Re_m \leq 100$, the friction factors for the simulations are larger than the corresponding values predicted by the KTA (1981) correlation. From the results shown in Figure 4.1-3, it can be concluded that the friction factors obtained from the simulations are a realistic representation of the resistance of the simulated BCC packed bed.

4.1.2 Discussion of the Wentz and Thodos (1963) mesh dependence study

As stated in Section 4.1.1, the pressure drops predicted by the simulations were used to calculate the friction factors according to the Blake (1922) correlation in Eq. (2.7). The friction factors were then compared to those calculated from the friction factor correlations proposed by Ergun (1952), Wentz and Thodos (1963), KTA (1981), and Eisfeld and Schnitzlein (2001) as well as the experimental friction factors obtained by Wentz and Thodos (1963). It was found that the friction factors calculated for all the meshes were in very close agreement to the friction factors calculated from the KTA (1981) correlation, as well as with the experimental friction factors obtained by Wentz and Thodos (1963).

In terms of the close agreement with the KTA (1981) friction factor correlation, it shows that the correlation is quite accurate for its given range of structural and flow parameters. Therefore, the KTA (1981) can be considered to be an accurate tool to predict the performance of a pebble bed reactor. The large difference between the simulation friction factors and the KTA (1981) correlation at $Re_m = 10$ is possible due to the inadequate resolution of the viscous sublayer over the spheres in the simulation, or it could be due to the KTA (181) correlation not taking the wall

effect into account. Reddy and Joshi (2010) found that correlations which include the influence of the wall effect on fluid flow through the bed tend to predict the friction factors more accurately. From the lower limit given by KTA (1981) for the applicability of the KTA (1981) correlation in Figure 2.3-1, the correlation is not applicable for $Re_m = 10$ and an aspect ratio of $\alpha = 11.38$. From the analyses performed by Van der Merwe (2014) and the improved lower limit proposed by Van der Merwe (2014) the KTA (1981) correlation will be applicable for $Re_m > 40$ for an aspect ratio of 11.38.

The close agreement of the simulation friction factors and the Wentz and Thodos (1963) experimental friction factors indicates that the methodology created to replicate the Wentz and Thodos (1963) physical experiments generates accurate representative results, despite the difference in porosity, bed length and fluid properties (namely temperature, ambient pressure, viscosity and density). Figure 4.1-3 shows good agreement between experimental, correlation and simulation values of Wentz and Thodos (1963).

4.2 PDTS Simulations

The objective of the PDTS simulations were to determine whether it would be possible to obtain results with CFD simulations which compare accurately with the experimental results of the PDTS tests for three of the experimental pressure levels: 4, 7 and 11, which were at 400 kPa, 700 kPa and 20000 kPa, respectively. The particle Reynolds number of the flows at pressure levels 4, 7 and 11 were $Re_p = 4000$, 7000 and 20000, respectively. The experimental pressure drops were measured between the inlet and outlet, and the friction factors were calculated from the experimental parameters according to the Blake (1922) friction factor correlation (Eq. (2.7)). The experimental pressure drop and dimensionless friction factors for the selected cases are shown in Table 4.2-1:

Table 4.2-1: PDTS Experimental pressure drops and friction factors

Pressure Level	Pressure drop (Pa)			Friction factor (-)		
	PDTS036	PDTS039	PDTS045	PDTS036	PDTS039	PDTS045
4	365.4	246.5	136.3	1.49	1.35	1.19
7	523.6	351.8	185.3	1.21	1.09	0.95
11	1021.9	672.4	342.4	0.80	0.71	0.60

From Table 4.2-1, it can be seen that the pressure drops measured at the same pressure level differed significantly between the porosities. For instance, the pressure drop measured for PDTS036 was 1021.9 Pa at pressure level 11, but it was only 342.4 Pa for PDTS045. This

difference could be due to a decrease in the tortuosity in the flow for the larger porosity, as well as a lower interstitial velocity associated with the larger porosity.

The PDTS beds were simulated according to the methodology established in Section 3.3. The predicted pressure drops as well as the friction factors calculated from Eq. (2.7) for each of the three porosities will be shown in the following sections. It should be noted that in Table 4.2-2 to Table 4.2-8, the term “Prism layer thickness” refers to thickness of the prism layers globally and over the spheres as a percentage of the base size.

4.2.1 PDTS036

The meshes that gave the most favourable results for the chosen pressure levels for PDTS036 are shown in Table 4.2-2. This bed has a porosity of $\epsilon = 0.351$, which included the cables between the spheres.

Table 4.2-2: Simulation friction factors calculated for flows at Pressure Levels 4, 7 and 11 for PDTS036

Pressure Level	Prisms layers	Prism layer thickness (%)		Pressure drop (Pa)	$\Psi_{StarCCM+}$	$\Psi_{Experimental}$	Ψ Error percentage (%)
		Global	Spheres				
4	5	20	10	173.86	1.417	1.494	-5.19
7	5	20	10	274.66	1.2678	1.2123	4.577
11	3	12.5	3.75	508.16	0.842	0.802	0.5

Table 4.2-2 shows the mesh settings, the pressure drop predicted by Star-CCM+ and the associated friction factors for PDTS036. From Table 4.2-2, it can be seen that the mesh that gave accurate results for pressure level 7 also generated accurate results for pressure level 4. It should be noted that the mesh resulted in an under-prediction of the pressure drop of 5% for pressure level 4, whilst it resulted in an over-prediction of the pressure drop for pressure level 7. It is also clear from Table 4.2-2 that a thicker prism layer area is more suited for the prediction of the pressure drop at lower Reynolds numbers ($Re_p \leq 7000$), where a thinner prism layer gave a very accurate prediction of the pressure drop at highly turbulent flows ($Re_p = 20000$). This indicates that the boundary layer over the spheres is much thinner at higher Reynolds numbers, becoming gradually thicker as the Reynolds number decreases.

4.2.2 PDTS039

The meshes that gave the most favourable results for the chosen pressure levels for PDTS039 are shown in Table 4.2-3. This bed has a porosity of $\epsilon = 0.389$, including the cables.

Table 4.2-3: Friction factors calculated for flows at Pressure Levels 4, 7 and 11 for PDTS039

Pressure level	Prisms layers	Prism layer thickness (%)		Pressure drop (Pa)	$\Psi_{StarCCM+}$	$\Psi_{Experimental}$	Ψ Error percentage (%)
		Global	Spheres				
4	7	30	30	110.064	1.197	1.346	-11.056
7	5	20	15	170.262	1.052	1.091	-3.526
11	3	15	5	334.56	0.709	0.714	-0.775

Table 4.2-3 shows the mesh settings, pressure drops predicted by Star-CCM+ and the associated friction factors for PDTS039. In comparison with PDTS036 in Table 4.2-2, slightly thicker prism layers were needed to adequately resolve the viscous sublayer and accurately predict the pressure drop at corresponding pressure levels. As with the PDTS036 simulations, more accurate results were obtained at the higher turbulent flows (pressure level 11) compared to the less turbulent flows at pressure level 4. This could be due to the wall effect being less pronounced at higher Reynolds numbers, as suggested by Eisfeld and Schnitzlein (2001). Furthermore, it can also be seen that the friction factor obtained at pressure level 4 differed by more than 10% from the experimental values despite the relatively thick prism layers. Although within the confidence levels of the KTA (1981) and Eisfeld and Schnitzlein (2001) (15% (KTA, 1981) and 31%, respectively (Eisfeld and Schnitzlein, 2001)) correlations, the aim of this study was to achieve error percentages of less than 10%.

4.2.3 PDTS045

The meshes that gave the most favourable results for the chosen pressure levels for PDTS045 are shown in Table 4.2-4. This bed has a porosity of $\epsilon = 0.448$, including the cables.

Table 4.2-4: Friction factors calculated for flows at Pressure Levels 4, 7 and 11 for PDTS045

Pressure Level	Prisms layers	Prism layer thickness (%)		Pressure drop (Pa)	$\Psi_{StarCCM+}$	$\Psi_{Experimental}$	Ψ Error percentage (%)
		Global	Spheres				
4	8	35	35	53.685	0.936	1.192	-21.433
7	6	25	25	85	0.869	0.949	-8.43
11	5	15	5	158.65	0.555	0.597	-7.083

Table 4.2-4 gives the mesh settings, pressure drops predicted by Star-CCM+ and the associated friction factors for PDTS045. Much thicker prism layers were needed to adequately resolve the

flow over the packed bed at the same pressure level compared to PDTS036 and PDTS039. For example, the prism layers had to be 20% and 66.7% thicker globally and over the spheres respectively than those for PDTS036 at pressure level 7. The larger required thickness for the prism layers at the same pressure levels suggest that the boundary layers are thicker for the larger porosities. As with PDTS039, it was not possible to obtain an accurate prediction for the friction factor for PDTS045 at pressure level 4, despite making use of a large mesh thickness and a large number of prism layers.

4.2.4 Additional PDTS simulations

Additional simulations were run for all three Pressure Drop Test Sections. The purpose of these simulations was to determine over what range of pressure levels (and therefore Reynolds numbers) the meshes still gave accurate results. Furthermore, the effect of various prism layer settings and turbulence models for modelling the flow at pressure level 4 for PDTS039 and PDTS045 were also investigated. The results for each Pressure Drop Test Section will be shown in separate tables.

4.2.4.1 PDTS036 Additional Simulations

It was decided to determine over what range the meshes could predict the pressure drop to a high degree of accuracy, and to determine the influence of the prism layers on the pressure drop. The simulations shown in Table 4.2-5 were performed for PDTS036.

Table 4.2-5: Additional pressure level simulations of PDTS036

Pressure Level	Prisms layers	Prism layer thickness (%)		Pressure drop (Pa)	$\Psi_{StarCCM+}$	$\Psi_{Experimental}$	Ψ Error percentage (%)
		Global	Spheres				
3	5	20	10	135.585	1.503	1.642	-8.5
9	5	20	10	341.496	1.218	1.10	10.606
9	5	15	7.5	331.086	1.181	1.10	-7.235
10	5	15	5	337.587	1.079	1.058	1.91
10	3	12.5	3.75	291.516	0.931	1.058	-11.99
14	3	12.5	3.75	1094.597	0.638	0.681	6.336

Table 4.2-5 shows the mesh settings, pressure drops predicted by Star-CCM+ and the associated friction factors for the additional simulations for PDTS036. The first two simulations are at pressure levels 3 and 9 and used the same mesh that gave accurate results for pressure levels 4 and 7 in Table 4.2-2. This shows that a mesh with 5 prism layers which has a global thickness

of 20% and a thickness of 10% over the bed can be used to accurately predict the pressure drop over $3000 \leq Re_p < 9000$.

It should be noted that the same mesh which calculated a very accurate pressure drop at pressure level 11 underpredicted the pressure drop at pressure level 10, but slightly overpredicted the pressure drop at pressure level 14. This shows that that the prism layers have a clear impact on the pressure drop.

4.2.4.2 PDTS039 Additional Simulations

The following additional simulations shown in Table 4.2-6 and Table 4.2-7 were performed for PDTS039:

Table 4.2-6: Additional simulation performed for PDTS039

Pressure Level	Prisms layers	Prism layer thickness (%)		Pressure drop (Pa)	$\Psi_{StarCCM+}$	$\Psi_{Experimental}$	Ψ Error percentage (%)
		Global	Spheres				
14	3	15	5	735.309	0.587	0.565	4.04

Table 4.2-6 shows the mesh settings, pressure drop predicted by Star-CCM+ and the associated friction factor. From Table 4.2-6, it can be seen that the mesh that gave accurate results at pressure level 11 for PDTS039 in Table 4.2-3 also gave accurate results at pressure level 14.

Furthermore, pressure level 4 was also simulated with the standard $k-\omega$ turbulence model with low-y^+ wall treatment, as well as LES with low-y^+ wall treatment, to determine if the pressure drop could be resolved more accurately. The chosen turbulence models, mesh settings, pressure drops predicted by Star-CCM+, and the associated friction factors for PDTS039 are shown in Table 4.2-7:

Table 4.2-7: Different turbulence models and wall treatments used to simulate the flow at pressure level 4 for PDTS039

Turbulence model	Prisms layers	Prism layer thickness (%)		Pressure drop (Pa)	$\Psi_{StarCCM+}$	$\Psi_{Experimental}$	Ψ Error percentage (%)
		Global	Spheres				
LES	10	35	35	108.774	1.183	1.347	-12.098
$k-\omega$	5	25	25	113.251	1.232	1.347	-8.482

From Table 4.2-7, it can be seen that in the case of the LES model that increasing the prism layer thickness from the values reported in Table 4.2-3 led to a slight decrease in the pressure drop

accuracy. This indicates that the mesh quality has most likely decreased. Furthermore, the combination of the standard Wilcox $k-\omega$, with low-y$^+$ wall treatment and a mesh with thinner and fewer prism layers predicted a pressure drop which was within the required error percentage range. This suggests that the applicability of the $k-\omega$ turbulence model should be investigated in more detail.

4.2.4.3 PDTS045 Additional simulations

Additional simulations were also performed for PDTS045. The flow at pressure level 14 was simulated, as well as the flow at pressure level 4. Table 4.2-8 shows the mesh settings, pressure drop predicted by Star-CCM+ and the associated friction factor at pressure level 14 for PDTS045:

Table 4.2-8: Additional simulation performed for PDTS045

Pressure level	Prisms layers	Prism layer thickness (%)		Pressure drop (Pa)	$\Psi_{StarCCM+}$	$\Psi_{Experimental}$	Ψ Error percentage (%)
		Global	Spheres				
14	5	15	5	336.318	0.443	0.448	-1.237

The mesh settings used for this simulation was also the mesh settings used to simulate the flow at pressure level 11 for PDTS045 as shown in Table 4.2-4. It can be seen from Table 4.2-8 that the result for pressure level 14 has a similar accuracy as that for pressure level 11 for PDTS045.

Furthermore, the flow at pressure level 4 was also simulated using a different turbulence model. As for the flow at pressure level 4 for PDTS039 in Table 4.2-7, the flow at pressure level 4 for PDTS045 was also simulated using the standard Wilcox $k-\omega$ wall turbulence model and low-y$^+$ wall treatment. The mesh settings, pressure drop predicted by Star-CCM+ and the associated friction factor for PDTS045 is shown in Table 4.2-9:

Table 4.2-9: Flow simulated at Pressure Level 4 for PDTS045 with Standard Wilcox $k-\omega$ turbulence and low-y$^+$ wall treatment

Pressure Level	Prisms layers	Prism layer thickness (%)		Pressure drop (Pa)	$\Psi_{StarCCM+}$	$\Psi_{Experimental}$	Ψ Error percentage (%)
		Global	Spheres				
4	5	25	25	57.421	0.969	1.192	-18.731

Although the error percentage was larger than the limit of 10% set for this study, this combination of turbulence model, wall treatment and prism layer settings predicted a value for the friction factor which represented a slight improvement compared to the corresponding value in Table 4.2-4.

4.2.5 Discussion of the PDTS results

The goal of this section was to determine whether it would be possible to use CFD to numerically simulate the experiments conducted on the Pressure Drop Test Sections (PDTS) with a high degree of accuracy. The Pressure Drop Test Sections consisted of three beds with porosities of $\epsilon = 0.36$, $\epsilon = 0.39$ and $\epsilon = 0.45$, with 30 layers of spheres in a body-centred cubic configuration. In the PDTS experiments, nitrogen was pumped through the different beds at different inlet pressure levels, from 100 kPa to 5000 kPa. The pressure levels were varied to vary the particle Reynolds numbers of the flow from $1000 \leq Re_p \leq 50000$, whilst keeping the superficial velocity approximately constant (Du Toit & Rousseau, 2014). In the simulations, various turbulence models, wall treatments and mesh settings were tested to determine their validity. The flow over the Pressure Drop Test Sections was simulated for three Pressure Levels and associated particle Reynolds numbers of $Re_p = 4000$, $Re_p = 7000$ and $Re_p = 20000$.

Three main turbulence models were tested to determine their validity: $k - \epsilon$, $k - \omega$ and LES. LES with all-y^+ wall treatment was eventually chosen to conduct the simulations. The reasoning behind these choices are given in Section 3.3. During testing, it was found that the number of prism layers and their respective thicknesses was of great importance when attempting to accurately predict the pressure drop. The prism layers resolve the viscous sublayer close to the regions defined as no-slip walls, which for the PDTS simulations were both the spheres in the packed bed and the containing wall. At less turbulent flows (pressure level 4) thinner prism layers lead to the pressure drop being underpredicted. Therefore, as the Reynolds number decreases, the viscous sublayer becomes thicker, and the thickness of the prism layers must be increased when the Reynolds number decreases.

For PDTS036 ($\epsilon = 0.36$), a mesh with 5 prism layers with a global thickness of 20% (of the base size) and a refined thickness of 10% over the bed generated accurate results at both pressure levels 4 and 7. A mesh with slightly fewer prism layers (3) with a reduced global and refined thickness (12.5% and 3.75%, respectively) was required to produce accurate results for pressure level 11, which had a higher level of turbulence compared to the flows at pressure levels 4 and 7.

The PDTS039 simulation meshes required slightly thicker prism layers at the same pressure levels as PDTS036. At pressure level 11 for PDTS039, the global and refined prism layer thickness had to be slightly increased to 15% and 5% respectively, to generate accurate results (an increase of 20% and 33.3% respectively in comparison to PDTS036). At pressure level 7, a mesh with 5 prism layers having a thickness of 20% globally and 15% over the bed generated very accurate results (3.96% deviation from experimental results).

Finding suitable mesh settings for PDTS045 proved to be very difficult. The highly turbulent flow at pressure level 11 could be accurately modelled with 5 prism layers with a global prism layer thickness of 15% and a refined prism layer thickness over the bed of 5%. Pressure level 7 required much thicker and more prism layers to resolve the viscous sublayer. The number of prism layers were increased to 6 and the prism layers had a global and refined thickness of 25%.

When considering the results obtained, it is apparent that as the pressure level of the flow increases, fewer and thinner prism layers are required to accurately model the flow through the beds. This can be ascribed to the viscous sublayer close to the spheres and the walls becoming thinner as the flow becomes more turbulent, and the wall effect becoming less pronounced for more turbulent flows (Eisfeld & Schnitzlein, 2001). It can also be seen that the same mesh that gave accurate results at pressure level 11 for each respective Pressure Drop Test Section also gave accurate results at pressure level 14. This may suggest that the viscous sublayer near the spheres might have reached a limit and thus does not become much thinner past a certain point. This means that the highly turbulent flows ($20000 \leq Re_p \leq 50000$) can be modelled with the same mesh.

As mentioned previously, the lengths of the simulated beds were half the lengths of the respective experimental beds and only a quadrant of the cross-section was modelled. When comparing the pressure drops for the specific pressure levels and beds from Table 4.2-1, and the corresponding values in Table 4.2-2 to Table 4.2-4, it can be seen that the simulated pressure drops are approximately half the values of the experimental pressure drops, which corresponds to the lengths of the simulated beds being half that of the experimental beds. In most cases the simulated friction factors are also in good agreement with the experimental friction factors. These results therefore justifies the choice to limit the simulated domain to an eighth of the geometry of the experimental beds.

It is also apparent that as the porosity increases, the prism layers need to be thicker to be able to simulate the flow with a sufficient degree of accuracy. This suggests that the viscous sublayer becomes thicker as the porosity increases. This increase in the viscous layer thickness can be linked to the interstitial velocity. As mentioned previously, the superficial velocity for all cases were approximately the same. This means that the interstitial velocity will decrease as the porosity increases. The comparison between the interstitial velocities for the different porosities at pressure level 11 is shown in Table 4.2-10:

Table 4.2-10: Comparison of interstitial velocities between the different Pressure Drop Test Sections

Pressure Drop Test Section	U_i $(m \cdot s^{-1})$
PDTS036	1.50921
PDTS039	1.40483
PDTS045	1.21362

It can be seen from Table 4.2-10 that the interstitial velocities decrease as the porosity increases. This would cause the local velocity to decrease when flowing through the bed because of the wider spacing between the spheres, which would cause an increase in the thickness of the viscous layer due to the slower moving fluid, which would require thicker prism layers to resolve the flow sufficiently. This explains the required increase in the prism layer thickness as the porosities of the beds increase. However, the prism layer thickness can only be increased up to a certain point before the mesh quality starts to decrease substantially due to the spatial limit imposed by the size of the gaps between the spheres.

Lastly, the flow at Pressure Level 4 for PDTS039 and PDTS045 could not be modelled accurately with the LES turbulence model and all-y^+ wall treatment. However, the Standard Wilcox $k-\omega$ turbulence together with low-y^+ wall treatment, in conjunction with thinner prism layers, gave a friction factor at Pressure Level 4 for PDTS039 which was within the desired error percentage range of less than 10%. This combination of wall treatment and turbulence model was chosen specifically due to its ability to better solve the viscous forces near the spheres and walls. However, the Standard Wilcox $k-\omega$ model is sensitive to the turbulence in the free-stream (CD-Adapco, 2012); and due to the lack of knowledge of the transition point from the viscous sublayer to the buffer and log-law layers, this model can be unstable when used at higher Reynolds numbers. It should also be noted that using these physics and mesh continua settings for the flow at Pressure Level 4 for PDTS045 did not produce accurate results.

CHAPTER 5: CONCLUSIONS

This chapter will discuss the conclusions reached from the Wentz and Thodos (1963) mesh dependence study and the analysis of the pressure drop over the Pressure Drop Test Section CFD simulations. Both parts of this study were conducted using the CFD program Star-CCM+ version 12. The flow through structured packed beds, which were generated in the CAD program SolidWorks 2016, was modelled accounting explicitly for the spheres.

5.1 Wentz and Thodos (1963) mesh dependence study

The aim of the Wentz and Thodos (1963) mesh dependence study was to determine the influence of mesh fineness on the pressure drop of air flowing through a body-centred structured packed bed. The methodology developed by Van der Merwe (2014) was used and further developed to improve the stability and convergence rate of the solution. The results of Van der Merwe (2014) obtained by using Star-CCM+ version 7 was found to be valid when using Star-CCM+ version 12. The bed developed by Van der Merwe (2014) in SolidWorks (2016) was found to be a good representation of the experimental beds used by Wentz and Thodos (1963), although it did differ in length and porosity. These structural differences were due to the improvement of the quality of the mesh at the contact points of the spheres. The flow was explicitly simulated by using the Realizable $k-\epsilon$ turbulence solver in a steady-state configuration.

The mesh dependence study was conducted by varying the base size of the mesh, and then testing the meshes over a wide range of particle Reynolds numbers. When conducting the mesh dependence study, it was found that the pressure drops predicted by both very fine and coarser meshes differed on average by 11.06%, with a maximum and minimum difference of 28% and 3.3%, respectively. When analysing the predicted pressure drops, it was found that for $Re_p < 4000$, the predicted pressure drop decreased with an increase in the base size, but for $Re_p \geq 4000$ the pressure drop increased with an increase in the base size.

Due to the relatively small variation in the results obtained for the various mesh base sizes, the pressure drop results were analysed statistically. It was found that the pressure drops predicted by both the meshes with base sizes of 15 and 20 mm respectively were consistently within one standard deviation from the mean. The base size of 20 mm was chosen as the most favourable base size, due to it generating results with the same accuracy as the mesh with base size of 15 mm, but with a slightly shorter solution time.

The friction factors calculated from the simulation pressure drops were found to be in close agreement with those obtained by Wentz and Thodos (1963) in their pressure drop experiments.

The simulation friction factors also compared well with those calculated from the friction factor correlations proposed by Wentz and Thodos (1963) and the KTA (1981) for most of the Reynolds numbers. However, at the lowest modified Reynolds number ($Re_m = 10$), the simulation friction factor was twice that predicted by the KTA (1981) correlation. This could be due to the fact that the KTA (1981) correlation does not account for the wall effect.

Overall, it can be concluded that the mesh dependence study was successful in that the influence of mesh fineness on the simulated pressure drops were determined. However, the behaviour of the pressure drop as a function of the base size appears to be affected by the flow regime and requires further investigation.

5.2 Pressure Drop Test Section Simulations

The aim of the Pressure Drop Test Section simulations was to investigate the validity of CFD to numerically model the experimental pressure drops over the PDTS beds. These beds had a body-centred cubic configuration and had porosities of $\epsilon = 0.351$, 0.389 and 0.448 respectively. The geometry of the bed used in the simulations had a cross-section a quarter the size of those used in the PDTS experiments, with half the number of sphere layers of the experimental beds. The flow was simulated at three pressure levels, which represented particle Reynolds numbers of $Re_p = 4000$, 7000 and 20000, and the LES turbulence model was used to model the mixing of the flow through the bed.

The first objective of this part of the study was to conduct a residual analysis to find favourable turbulence and wall treatment settings which would sufficiently lower the residuals and allow for convergence of the solver. In this regard, the methodology of Vermaak (2019) was used and improved upon. The LES turbulence model was chosen in conjunction with all-y^+ wall treatment, and the segregated solver was used. This combination proved to be stable and converged smoothly.

The original assumption was that the mesh continua parameters could be chosen in such a way that the flow could be accurately modelled over the entire range of particle Reynolds numbers and porosities. However, it was found that the mesh continua parameters had to be chosen individually for the flow at each pressure level for each porosity. The mesh continua parameters that proved to be the most important in terms of the pressure drop over the bed was found to be the number of prism layers and the thickness of the prism layers in terms of the base size. Also, it was assumed that the cables which were used to maintain the distances between the spheres in the experimental beds had a negligible influence on the pressure drop. However, the

simulations revealed that this was not so, and the cables had to be included in the geometry to produce accurate results.

Testing revealed that to accurately predict the pressure drop at the lower Reynolds numbers ($Re_p \leq 7000$), more and thicker prism layers were required, otherwise the pressure drop was underpredicted. As the Reynolds number increased, the number and thickness of the prism layers required needed to be reduced. Also, it was noted that the flow at the same pressure level also required thicker and more prism layers to accurately predict the pressure drop as the porosity increased. Therefore, the prism layers were much thicker at pressure level 7 for $\epsilon = 0.448$ than for $\epsilon = 0.351$.

The thicker prism layers required to model the flow at lower Reynolds numbers could be explained by the increase in the thickness of the viscous boundary layer that forms close to the spheres and containing walls, which would require more prims layers to accurately resolve. Also, as the porosity of the bed increases, the interstitial velocity decreases. If the interstitial velocity decreases, the viscous sublayer becomes thicker and has an increasing impact on the pressure drop.

All flows at every pressure level for each porosity could be solved so that the simulated friction factors came within 10% of the experimental friction factors. However, the flow at pressure level 4 for $\epsilon = 0.389$ (PDTS039) and $\epsilon = 0.448$ (PDTS045) could not be accurately modelled, even when using thicker prism layers. However, the flow at pressure level 4 for PDTS039 could be accurately modelled using the Standard Wilcox $k - \omega$ and low-y^+ wall treatment.

It should be noted that although the thickness of the prism layers can be further increased, but the quality of the mesh cells between the spheres will dramatically decrease due to the spatial limit imposed by the size of the gaps between the spheres.

Therefore, the conclusion was reached that it is possible to accurately model the flow over the Pressure Drop Test Sections using CFD for certain porosities and flow conditions, but not all. It can be concluded that although it can be said that the PDTS experiments can be modelled using CFD, further study is required to develop an understanding of the relationship between the mesh settings and the flow conditions to be able to obtain accurate solutions.

5.3 Recommendations

Several recommendations are proposed for both the Wentz and Thodos (1963) mesh dependence study and the Pressure Drop Test Section CFD validation simulations.

5.3.1 Wentz and Thodos (1963) Mesh Dependence Study Recommendations

The following points for the Wentz and Thodos (1963) mesh dependence study are recommended to be investigated further:

- It is recommended that the effect that the flow conditions have on the behaviour of the pressure drop as function of base size, should be investigated further.
- From the PDTS simulations, Standard Wilcox $k-\omega$ turbulence proved to be a viable option for flows which produce a thicker viscous sublayer, such as low Reynolds number flows or flows with lower interstitial velocities. It is recommended that its suitability for the Wentz and Thodos (1963) beds also be investigated.
- Additionally, the influence that additional and thicker prism layers will have on the mesh quality and pressure drop can also be investigated further.

5.3.2 PDTS CFD Validation Recommendations

The following recommendations are made for further investigation into the PDTS CFD validation simulations:

- The influence that the prism layers have on the pressure drop and accuracy of the flow was noted, but not fully explored. It is recommended that further investigations be conducted into the influence of the prism layers as well as the formation of the flow sub-layers close to the spheres.
- Large Eddy Simulations were chosen as the turbulence model due to the instability of Eddy Viscosity models at higher Reynolds numbers. However, the applicability of other turbulence models, such as the Reynolds Stress Models, was not tested due to time constraints. It is recommended that further investigation should be conducted into the applicability of other turbulence models.
- The viscous sublayers which form close to the spheres proved to have a strong influence on the pressure drop. The flow at a particle Reynolds number of $Re_p = 1000$ (Pressure Level 1) for PDTS036 could also not be modelled accurately with LES, although it did fall outside the scope of this investigation. It is interesting to note that the experimental pressure drop at Pressure Level 1 for PDTS036 was the same as the experimental pressure drop at Pressure Level 4 for PDTS045, which could also not be solved with the LES turbulence model. Therefore, it is recommended that the influence of viscous forces near the walls and spheres should be further investigated.

BIBLIOGRAPHY

Abou-Sena, A. et al., 2013. Experimental study and analysis of the purge gas pressure drop across the pebble beds for the fusion HCPB blanket. *Fusion Engineering and Design,* Volume 88, pp. 243-247.

Achenbach, E., 1995. Heat and Flow Characteristics of Packed Beds. *Experimental Thermal and Fluid Science,* Volume 10, pp. 17-27.

Atmakidis, T. & Kenig, E. Y., 2009. CFD-based analysis of the wall effect on the pressure drop in packed beds with moderate tube/particle diameters in the laminar flow regime. *Chemical Engineering,* Volume 59, pp. 404-410.

Bai, H., Theuerkauf, J. & Gillis, P. A., 2009. A Coupled DEM and CFD Simulation of Flow Field and Pressure Drop in Fixed Bed Reactor with Randomly Packed Catalyst Particles. *Industrial & Engineering Chemistry Research,* Volume 48, pp. 4060-4074.

Baker, T. J. & Tabor, G. R., 2010. Computational analysis of transitional air flow through packed columns of spheres using the finite volume technique. *Computers and Chemical Engineering,* Volume 34, pp. 878-885.

Blake, F., 1922. The resistance packing to fluid flow. *Transactions of the Institution of Chemical Engineers,* Volume 14, pp. 415-421.

Calis, H. P. A. et al., 2001. CFD modelling and experimental validation of pressure drop and flow profile in a novel strucutured catalytic reactor packing. *Chemical Engineering Science,* Volume 56, pp. 1713-1720.

Caulkin, R. et al., 2007. An investigation of sphere packed shell-side columns using a digital packing algorithm. *Computers and Chemical Engineering,* Issue 31, pp. 1715-1724.

CD-Adapco, 2012. *STAR-CCM+ User Guide.* 7 ed. s.l.:s.n.

De Klerk, A., 2003. Voidage Variation in Packed Beds at Small Column to Particle Diameter Ratio. *American Industrial & Chemical Engineering Journal,* 49(8), pp. 2022-2029.

Di Felice, R. & Gibilaro, L., 2004. Wall effects for the pressure drop in fixed beds. *Chemical Engineering Science,* Volume 59, pp. 3037-3040.

Du Toit, C. G., 2008. Radial variation in porosity in annular packed beds. *Nuclear Engineering and Design,* Volume 238, pp. 3073-3079.

Du Toit, C. G. & Rousseau, P. G., 2014. *Separate Effects Tests to Determine the Pressure Drop over Packed Beds in the PBMR HPTU Test Facility.* Weihai, HTR 2014.

Du, W. et al., 2015. Experimental and statistical analysis of the void size distribution and pressure drop validations in packed beds. *Chemical Engineering Research and Design,* Issue 106, pp. 115-125.

Eisfeld, B. & Schnitzlein, K., 2001. The influence of confining walls on the pressure drop in packed beds. *Chemical Engineering Science,* Volume 56, pp. 4321-4329.

Eppinger, T., Seidler, K. & M, K., 2011. DEM-CFD simulations of fixed bed reactors with small tube to particle diameter ratios. *Chemical Engineering Journal,* Volume 166, pp. 324-331.

Erdim, E., Akgiray, Ö. & Demir, I., 2015. A revisit of pressure drop-flow rate correlations for packed beds. *Powder Technology,* Issue 283, pp. 488-504.

Ergun, S., 1952. Fluid flow through packed columns. *Chemical Engineering Progress,* 48(2), pp. 89-94.

Handley, D. & Heggs, P., 1968. Momentum and heat transfer mechanisms in regular shaped packings. *Trans. Inst. Chem. Eng.,* Volume 46, pp. 251-254.

Hassan, Y. A., 2008. Large eddy simulation in pebble bed gas cooled core reactors. *Nuclear Engineering and Design,* Issue 238, pp. 530-537.

Hassan, Y. A. & Kang, C., 2012. *Pressure drop in a pebble bed reactor under high Reynolds number,* College Station: Texas A&M University.

Hicks, R. E., 1970. Pressure Drop in Packed Beds of Spheres. *Industrial & Engineering Chemistry Fundamentals,* 9(3), pp. 500-502.

KTA, 1981. *Safety Standards of the Nuclear Safety Standards Commision (KTA),* Salzgitter: KTA.

Latifi, M. S. & Du Toit, C. G., 2019. A Numerical Study to Investigate the Effect of Inlet Reynolds Number on the Thermal-Fluid Phenoma in the Supercritical Carbon Dioxide-Cooled Pebble Bed Reactor. *Arabian Journal for Science and Engineering,* Issue 44, pp. 981-991.

Latifi, M. S. & Saeed, S., 2016. Effects of porosity on thermal-fluid phenomena in PBMR core. *Journal of Thermal Engineering,* 2(4), pp. 853-860.

Lopes, R. J. G. & Quinta-Ferreira, R. M., 2008. Three-dimensional numerical simulation of pressure drop and liquid holdup for high-pressure trickle-bed reactor. *Chemical Engineering Journal,* Volume 145, pp. 112-120.

Mehta, D. & Hawley, M. C., 1969. Wall Effect in Packed Columns. *Industrial & Engineering Chemical Process Design and Development,* 8(2), pp. 280-282.

Munson, B. R., Okiishi, T. H., Huebsch, W. W. & Rothmayer, A. P., 2013. *Fluid Mechanics.* 7th ed. Singapore: Wiley.

Peric, M. & Ferguson, S., 2008. *The advantage of polyhedral meshes.* [Online]
Available at:
https://pdfs.semanticscholar.org/51ae/90047ab44f53849196878bfec4232b291d1c.pdf
[Accessed 11 October 2019].

Preller, A. C. N., 2011. *Numerical modelling of flow through packed beds of uniform spheres,* Potchefstroom: North-West University.

Raichura, R., 2010. Pressure drop and heat transfer in packed beds with small tube-to-particle diameter ratio. *Experimental Heat Transfer: A Journal of Thermal Energy Generation, Transport, Storage and Conversion,* 12(4), pp. 309-327.

Reddy, R. K. & Joshi, J. B., 2008. CFD modeling of pressure drop and drag coefficient in fixed and expanded beds. *Chemical Engineering Research and Design,* Volume 86, pp. 444-453.

Reddy, R. K. & Joshi, J. B., 2010. CFD modeling of pressure drop and drag coefficient in fixed beds: Wall effects. *Particuology,* Volume 8, pp. 37-43.

Ribeiro, A., Neto, P. & Pinho, C., 2010. Mean Porosity and Pressure Drop Measurements in Packed beds of Monosized Spheres: Side Wall Effects. *International Review of Chmeical Engineering,* 2(1), pp. 40-46.

Rose, H. E., 1945. An Investigation into the Laws of Flow of Fluids through Beds of Granular Materials. *Proceedings, Institution of Mechanical Engineers,* Volume 153, pp. 141-148.

Rousseau, P. & van Staden, M., 2008. Introduction to the PBMR heat transfer test facility. *Nuclear Engineering and Design,* Issue 238, pp. 3060-3072.

Seguin, D., Montillet, A. & Comiti, J., 1998. Experimental characterisation of flow regimes in various porous media - I: Limit of Laminar flow regime. *Chemical Engineering Science,* 53(21), pp. 3751-3761.

Suekane, T., Yokouchi, Y. & Hirai, S., 2003. Inertial Flow Structures in a Simple-Packed Bed of Spheres. *American Industrial and Chemical Engineering Journal,* 49(1), p. 2003.

Susskind, H. & Becker, W., 1967. Pressure Drop in Geometrically Ordered Packed beds of Spheres. *American Industrial and Chemical Engineering Journal,* 13(6), pp. 1155-1159.

Tallmadge, J., 1970. Packed Bed Pressure Drop - An Extension to Higher Reynolds numbers. *AIChE,* 16(6), pp. 1092-1093.

Van Antwerpen, A., du Toit, C. G. & Rousseau, P. G., 2010. A review of correlationsto model the packing structure and effective thermal conductivity in packed beds of mono-sized spherical particles. *Nuclear Engineering and Design,* Issue 240, pp. 1803-1818.

Van der Merwe, W. J. S., 2014. *Analysis of flow through packed beds with small cylinder to particle ratios,* Potchefstroom: North-West University.

Van der Walt, A. J. K., 2006. *Pressure drop through packed beds,* Potchefstroom: Nort-West University Potchefstroom Campus.

Vermaak, H. J., 2019. *CFD analysis of thermal dispersion in a structured pebble bed,* Potchefstroom: North-West University.

Versteeg, H. K. & Malalasekera, W., 2007. *An Introduction to Computational Fluid Dynamics.* 2nd ed. Essex: Pearson Education Limited.

Vollmari, K., Oschmann, T., Wirtz, S. & Kruggel-Emden, H., 2015. Pressure drop investigations in packings of arbitrary shpaed particles. *Powder Technology,* Volume 271, pp. 109-124.

Wentz, C. A. & Thodos, G., 1963. Pressure Drops in the Flow of Gases Through Packed and Distended Beds of Spherical Particles. *A.I.Ch.E. Journal,* 9(1), pp. 81-84.

Winterberg, M. & Tsotsas, E., 2000. Impact of Tube-to-Particle-Diameter Ratio on Pressure Drop in Packed Beds. *AIChE,* 46(5), pp. 1084-1088.

Yang, J., Wang, Q., Zeng, M. & Nakayama, A., 2010. Computational study of forced convective heat transfer in structured packed beds with spherical or ellipsoidal particles. *Chemical Engineering Science,* Volume 65, pp. 726-738.

Ziólkowska, I. & Ziólkowski, D., 1988. Fluid flow inside packed beds. *Chemical Engineering Process,* Volume 23, pp. 137-164.